Strongly Interacting Systems: expanding sources in ultrarelativistic nuclear and hadronic collisions

DISSERTATION
zur
Erlangung des Doktorgrades
der Naturwissenschaften
(Dr. rer. nat.)

dem
Fachbereich Physik
der Philipps-Universität Marburg
vorgelegt von

Nelmara Arbex
aus São Paulo-SP, Brasilien

Marburg/Lahn 1997

Vom Fachbereich Physik der Philipps-Universität
als Dissertation am 10.07.1997 angenommen.

Erstgutachter: Prof.Dr. R. M. Weiner
Zweitgutachter: Prof. Dr. W. Kerler

Tag der mündlichen Prüfung: 17.07.97

Contents

PART II : Hadronic Collisions and the Expanding Source Model

Introduction

Our contemporary physical knowledge about the universe has lead us to the conclusion that there are in Nature only four kinds of interactions: the gravitational, the electromagnetical, the weak and the strong interaction. In this dissertation I will focus on the fourth one.

The interaction and resulting motions of very large objects such as the sun, earth and moon are essentially governed by the gravitational force. The everyday life on our planet is dominated by it. The electromagnetic force acts on all particles carrying electric charge and it is responsible for atomic and molecular structure of matter. The weak interaction is present only at the nuclear level and is responsible for a class of phenomena typified by the β radioactive decay of certain nuclei. The fourth interaction appears between particles called *hadrons*. This interaction acts on a very deep level in their structure - the quark level. It is responsible for binding the nuclear constituents and probably also holds the quarks within the nucleons.

The latter three forces are present at the nuclear and sub nuclear level. Despite the fact that we have not discovered any sign of the gravitational field in the nucleus, it is the only known many particle system where all forms of interactions could appear, meaning the unique possibility to study the connections between all interactions.

From the information we acquired during the last decades of high energy physics we can conclude: all hadrons are made of fundamental parts - quarks and gluons (partons) - and their interaction can be described by Quantum Chromodynamics (QCD). Quarks and gluons have color-charge.

The electromagnetic and the weak interactions are described by the electroweak dynamics. Electroweak dynamics and QCD together form the standard model of high energy physics. The standard model continues to be confirmed by the experiments, but there are still many mysterious aspects . Hadronization, the phase where hadrons are formed from partons, is not accessible for present-day QCD calculations. In the region where perturbative QCD is applicable, at large momentum transfer region, the partons are weakly coupled. This state of the matter is called quark gluon plasma. The phase transition of the matter from a quark gluon plasma to a hadronic phase could be of first or second order.

The theory predicts that the state where quarks and gluons are free should be 10^{15} times denser than iron and 10^{9} times hotter than the

surface of the sun. Such energy densities and temperatures could be created in Black Holes, in the center of some stars and at the beginning of our universe some microseconds after the Big Bang. This understanding of strong interaction is connected to questions about nucleosynthesis, dark matter, scale and structure of the universe. On our planet the only possibility to investigate this state and this theory is in laboratory.

The start of experiments in the high energy accelerators opened the possibility to create the quark gluon plasma (particularly in heavy ions collisions) and to check our models and theory about this intriguing aspect of Nature, looking for a description of nuclear matter in its fullness, its equation of state.

Since QCD does not yield a full understanding of the multiparticle production process, phenomenological methods are all we have to gain insight into the world of the fourth interaction. This study is a journey into this world.

In the present dissertation I will use two phenomenological models to analyze data from high energy physics experiments. These models are based on space-time description of the particle sources, which are the fireballs formed after the moment of the collision.

In Part I **heavy ions collisions** at high energies will be investigated using a relativistic hydrodynamical model. The model version I present here - HYLANDER-PLUS - is based on a previous model, which was developed in the Theoretical High Energy Physics group at Marburg University. It solves the relativistic hydrodynamical equations in an exact (3+1) dimensional numerical way. The first version was used to describe some experiments and offered a wide description of the data, opening the possibility for a general interpretation of processes involving strong interactions. But the early version had some limitations with regard to initial conditions, to the type of equation of state used to solve the hydrodynamical equations and to spectra calculations. These limitations are an obstacle to the simulation of the new data/experiment generation and to the development of a more amplified analysis. In the new model these limitations have been removed and the abilities for simulations of the first version have been maintained.

Using the new version I simulated four kinds of experiments (symmetric and asymmetric collisions), in different energy ranges, with different amounts of stopping. It is possible to restrict the free parameters to the ones in the equation of state creating a method to verify the phase transition influence on the data and on proposed QGP signatures. I calculate the production and spectra of 16 types of hadrons (Chapter 4) and contribute to clarify some experimental features of the data which have been misinterpreted before (Chapter 5). Photon production has

also been investigated (Chapter 6).

The possibility to analyze many new aspects of the data could open many new routes to be explored in the area of heavy ion physics (Chapter 7).

This first part represents the central focus of this study.

In Part II we turn our attention to **hadronic collisions** at high energies. I also use a phenomenological model and an expansion concept to describe the particle source, based on the quantum statistics and quantum optics principles. Here I am particularly interested in describing an aspect of data, which was not discussed in the first part: Bose-Einstein correlations.

The analysis of correlations data is the most promising possibility to get information about the sizes and lifetimes of the fireballs formed in such reactions. The precise interpretation of these data is fundamental in the description of the dynamics of strongly interacting matter. New higher order pion correlations data (third, fourth, fifth order) opened an interesting discussion in the scientific community about the validity of theoretical instruments to be used in the data analysis. This work could contribute to this discussion.

Chapter 1
The Theoretical Status

The only theory we have for the strong interaction has some special features which determine and restrict our view of this world of interactions. Its limitations compel the physicists to use phenomenological models to complete the scenario.

In this chapter I will give an overview about the last results and limits of Quantum Chromodynamics (QCD) in Section 1 and introduce the most important phenomenological models used to study heavy ions collisions in Section 2.

1 The QCD Results and Limits

The attempt to derive interactions in high energy physics from first principles (from a lattice gauge theory) and predict the behaviour of hadronic matter at finite temperature is very ambitious. There is no analytical method known which allows us to start from the lagrangian of QCD and obtain quantitative results for the whole temperature range and general physical conditions. Therefore one possibility is to use extensive numerical Monte Carlo simulations (statistical QCD).

1.1 Characteristics and predictions

This non-abelian gauge theory presents some special characteristics:

1. At high energy (at short distances and large momentum transfer), the effective coupling constant (α_c) decreases logarithmically, i. e. quarks and gluons appear to be weakly coupled. This is called quark deconfinement and characterizes the existence of a new phase of the matter: the Quark Gluon Plasma (QGP).

2. At large distances or small momentum transfer, the effective coupling becomes strong, it is interpreted as quarks and gluons are bound by the strong force (confined) into hadrons. This sector is not accessible to QCD standard calculations as the value of α_c is too large to compute series with reducing terms in perturbative methods.

3. At low energy, the QCD vacuum should be characterized by 'vacuum condensates' (as the quark condensate and the gluon condensate). The quark condensate describes the density of quark-antiquark pair in the vacuum. The physical picture is that the quarks acquire an effective mass through the interactions between themselves and the physical vacuum (broken chiral symmetry). By increasing the energy density (by increasing temperature or matter density), a phase transition could occur to the QGP, where partons are deconfined and chiral symmetry is approximately restored.

In summary, two essential predictions resulted from these studies: quark deconfinement and chiral symmetry restoration.

There are reasons to expect that the transition between the low and the high temperature is not smooth but exhibits a discontinuity [1]-[4]. This phase transition is expected to occur in a temperature range $150 < T_c < 220\ MeV$ and could be of first or second order [1].

According to the standard cosmological model [7], the temperature of the cosmic background radiation exceeded 200 MeV during the first 10 μs after the Big Bang. If the theoretical calculations are right, the early universe was, therefore, filled with a quark gluon plasma, rather than hadrons.

1.2 Status of lattice calculations

For technical reasons, the physical case (two nearly massless and one massive quark) is the most difficult to simulate. Improvements of the original algorithms and the increase of computing power have permitted better evaluations of many interesting quantities. The simulations have mainly been done for the cases: pure gluonic matter ($N_f = 0$), four degenerated flavors ($N_f = 4$) and two (or three) ($N_f = 2$ or $2 + 1$) flavors matter. The last case is nearer to the physical situation [8].

Present results indicate a smooth cross-over between phases for $N_f = 2$ light quark flavors and a first-order phase transition for $N_f \geq 3$.

2 Phenomenological Models

Thermodynamical concepts seems to constitute the natural language for the description of this strong interacting many particle world under

[1] The order of the chiral phase transition is believed to be quite sensitive to the number of light, dynamical quark flavors. The authors of [5] and [6] predict a second-order phase transition for two massless flavors and a first-order phase transition for three massless flavors.

extreme conditions but the applicability of these concepts has to be checked and verified. As a part of this procedure, other kinds of microscopical calculations have been used.

The use of thermodynamical concepts is also dependent on the thermal equilibration of the system [2]. Parton cascade models are used to describe the system in the pre-equilibrium stage. I cite them in Subsection 1.

In Subsection 2 the relativistic microscopic models are briefly presented. Subsection 3 contains an overview of the relativistic hydrodynamical models.

2.1 Parton cascade models

The cascade model of parton scattering [9] or the breaking of color-flux-tubes [10, 11] provide the basis for the first ideas about the mechanism of energy deposition.

Detailed microscopic models have been constructed [12, 13, 14] since that time. These models are based on the concept that the colliding nuclei can be decomposed into their parton substructure. The perturbative interaction of these partons can be followed almost until thermalization. It permits the study of energy deposition process in space-time and in momentum space in the framework of perturbative QCD.

Parton cascade models predict a very rapid thermalization of the deposited energy, in agreement with QCD calculations. The thermalized parton plasma is initially gluon rich and depleted of quarks [15]. How long it would take until the parton plasma reaches chemical equilibration is not yet clear.

2.2 Relativistic microscopic models

Monte Carlo codes based on String Models are widely used (see Quark Matter Conference Proceedings) to simulate and analyze heavy ion reactions. They are VENUS [16], MCFM [17], FRITIOF [18], IRIS [19], ATTILA [20], QGSM [21], HIJET[22], HIJING [23] and RQMD [24, 25]. They are all based on the ideas of string formation and fragmentation and are all non-plasma models.

The method proposed by these models to describe the phenomenology of heavy ion collisions is 'extrapolation': comparing the results of the experiments with results from known regions of high energy interactions, discriminating 'new physics' from the 'background' [26].

[2] QCD predicts that, in order to reach temperatures far above T_c, the initial kinetic energy of the nuclei must be rapidly thermalized on a time scale of order 1 fm/c.

The mechanism of string formation is different in the various models. Color exchange, momentum exchange (longitudinal excitation), among others, are the most used approaches. There are also different prescriptions to break the strings into smaller pieces (hadrons).

The calculated observables from the various models are very similar, because of the similarities in their formalisms [27]. Nevertheless, if the models include rescattering of secondary particles, differences between their results can emerge. Most models, which include rescattering, parametrize it with a single parameter determined from comparison with experimental data. RQMD includes measured cross-section and decay probabilities to do the parametrization. VENUS, QGSM and RQMD include rescattering of all particles.

2.3 Relativistic hydrodynamical models

The idea to use a hydrodynamical model to simulate nuclei collisions is not new and is based on a generalization of statistical models introduced by Pomeranchuck and Landau forty years ago [28]-[32].

A hydrodynamical approach is valid under the following conditions:
a) large number of degrees-of-freedom in the system.
b) small mean-free-path (compared with the dimensions of the system).
c) large amount of kinetic energy lost per parton collision.
d) short De-Broglie wave-length (compared with dimensions of the system).
e) the system is (locally) thermalized.

The condition a) is clearly fulfilled in a nucleus-nucleus collision especially if big nuclei are involved.

The mean-free-path depends on particle density and total cross section ($\lambda = 1/\rho\sigma$). The hot nuclear matter [3] has densities of, at least, $1/fm^3$ and the cross section for proton-proton reaction at 5 GeV laboratory energy is approximately 4 fm^2. The mean-free-path of a nucleon can be evaluated as 0.25 fm, fulfilling also condition b).

About condition c), the loss of kinetic energy per collision [4] has been measured in $p - A$ reactions and is about 50% [34, 35].

The De-Broglie wave-length is defined as $\lambda_B = h/p$ (p: momentum). It is a criterion to use quasi-classical approximations in a quantum system. For a pion with 1 GeV momentum this quantity is 1.2 fm, and thus smaller than the system dimensions.

[3] The nuclear density of 'normal' nuclear matter is estimated to be $0.17/fm^3$.

[4] In [33] the author showed that, in fact, only few collisions are enough to equilibrate momentum distributions in low energies nucleus-nucleus collisions.

There is some discussion about the fulfilment of condition e). Pre-equilibrium calculations using parton cascade models predict a very rapid thermalization ($\sim 1fm/c$), but we are not yet able to answer this precisely.

There are different variants of relativistic hydrodynamical models used in the attempt to simulate the realized experiments. One could try to classify the most important of them through the number of fluids used to describe the relativistic hydrodynamical reaction. There are one-fluid-dynamic models [36] - [42] and there are multi-fluid-dynamic models [43] - [46]. The possibility "to handle with very displaced momentum distributions of target and projectile nucleons" motivated the creation of the second kind of models [47]. HYLANDER is a model which can be used as a two-fluid model, when we are considering transparence in the reaction, and as a one-fluid model when we use the full-stopping option for the initial condition (For details, see Chapter 2 and 3).

There are differences between the above quoted models related to: initial conditions for the simulation; freeze-out criterions; equations of state to be used to solve the relativistic hydrodynamical equations and the precision of the codes to solve these equations. The above mentioned characteristics of the simulations will determine the limitations of the models in the choice of the experiments for simulation and in the calculation of the diverse aspects of particle production. They will also determine the quality of their conclusions.

There are many works where relativistic hydrodynamical models have been used to analyze several aspects of heavy ion collisions, but only few of them present comparisons with experimental data on particle spectra.

In [38] the negative hadrons spectra from $S + S$ (SPS) reaction is analyzed [5], this is also made in [42]. In [41] a study on proton spectra for $Au + Au$ (AGS) reaction is presented in comparison with experimental results. Photon production and negative hadrons production data are used in [48] for $S + S(SPS)$, $Pb + Pb(SPS)$, $S + Au(SPS)$ and $Au + Au(AGS)$ reactions. The reaction $S + Au(SPS)$ has been simulated and the calculation on negative hadrons, Λ, $\bar{\Lambda}$, K^0 and proton production was compared with available data in [49].

The results obtained using HYLANDER and HYLANDER-PLUS in the simulation of different reactions and the comparison of the calculations with experimental data will be presented in this dissertation.

[5] These results have been used later by the authors to analyze Bose-Einstein correlations for pions. Correlations data is not subject of the Part I of this dissertation.

References

[1] M. A. Pochodzalla, Ann. Rev. Nucl. Part Sci. 33 (1983) 199.

[2] J. C. Collins and M. Perry, Phys. Lett. 75 (1995) 1040.

[3] A. M. Polyakov, Phys. Lett. B72 (1977) 224.

[4] J. Polonyi, hep-ph/9509334.

[5] R. D. Pisarski and F. Wilczek, Phys. Rev. D29 (1984) 338.

[6] K. Rajagopal and F. Wilczek, Nucl. Phys. B399 (1993) 395.

[7] E. Kolb and M. S. Turner, 'The Early Universe', Ed. Eddison- Wesley, 1990.

[8] B. Peterson, Nucl. Phys. A525 (1991) 237c.

[9] R. K. Anishetty, P. Koehler and L. McLerran, Phys. Rev. D22 (1980) 2793.

[10] A. Bialas and W. Czyź, Phys. Rev. D31 (1985) 198.

[11] K. Kajantie and T. Matsui, Phys. Lett. B164 (1985) 373.

[12] K. Geiger and B. Muller , Nucl Phys. B369 (1992) 600.

[13] K. Geiger, Phys. Rep. 258 (1995) 237.

[14] K. J. Eskola and X. N. Wang, Phys. Rev. D49 (1994) 1284.

[15] E. Shuryak, Phys. Rev. Lett. 68 (1992) 3270.

[16] K. Werner, Phys. Rev. Lett 62 (1989) 2460.

[17] J. Ranf, Z. Phys. 43 (1989) 439.

[18] B. Anderson, G. Gustafson and B. Nilsson-Almquist, Nucl. Phys. B281 (1987) 289.

[19] T. P. Pansart, Nucl. Phys. A461 (1987) 521c.

[20] M. Gyulassy, preprint CERN/TH-4794/87.

[21] N. S. Amelin, K. K. Gudima and V. D. Toneev, Phys. Lett. B216 (1989) 473.

[22] A. Shor and R. Longacre, Phys. Lett. B218 (1989) 100.

[23] X. Wang and M. Gyulassy, Berkeley preprint LBL-29390.

[24] H. Sorge, H. Stoecker and W. Greiner, Nucl. Phys. A498(1989) 567c.

[25] H. Sorge et al., Z. Phys. C47 (1990) 629.

[26] H. R. Schmidt and J. Schukraft, Int. Jour. Mod. Phys G

[27] T. C. Awes and S. P. Sorensen, Nucl. Phys. A498 (1989) 123c.

[28] L. D. Landau; Izv. Akad. Nauk. (URSS) 17 (1953) 51.

[29] Collected Papers of Landau; Pregamon Press, London (1965), paper number 88.

[30] I. Y. Pomeranchuck; Dokl. Akad. Nauk. (URSS) 78 (1951) 889.

[31] S. Z. Belenkij and L. D. Landau; Fiz. Nauk. 56 (1955) 309.

[32] S. Z. Balenkij and G. A. Milekin; Zh. Eksp. Theor. Fiz. 29 (1955) 20; Sov. Phys. JEEP 2 (1976) 14.

[33] S. Nagamyia et al., Phys. Rev. C24 (1981) 971.

[34] W. Busza and A. S. Goldhaber, Phys. Lett B139 (1984) 235.

[35] J. Hüfner and A. Klar, Phys. Lett. B145 (1984) 167.

[36] T. L. McAbee, J. R. Wilson, J. A. Zingman, C. T. Alonso; Mod. Phys. Lett. A4 (1989) 983

[37] N. S. Amelin et al.; Phys. Rev. Lett. 67 (1991) 1523.

[38] E. Schnedermann and U. Heinz; Proceedings of Workshop on Relativistic Heavy Ion Physics (1991) pg. 138.

[39] B. Waldhauser et al.; Z. Phys. C54 (1992) 459.

[40] D. Strottman, Nucl. Phys. A566 (1994) 245c.

[41] L. V. Bravina, N. S. Amelin, L. P. Csernai, P. Levai and D. Strottman; Nucl. Phys. A566(1994) 461c.

[42] R. Venugopalan, M. Prakash, M. Kataja and P. V. Ruuskanan; Nucl. Phys. A566 (1994) 473c.

[43] A. A. Amsden, A. S. Golhaber, F. H. Harlow and J. R. Nix; Phys. Rev. C17 (1978) 2080.

[44] L. P. Cernai et al.; Phys. Rev. C26 (1982) 149.

[45] I. N. Mishutin, V. N. Russkikh and L. M. Starov; Int. Rev. Mod. Phys. 5, World Scientific, Singapore (1991) 180.

[46] U. Katscher et al., Z. Phys. A346 (1993) 209.

[47] D. H. Rischke, S. Bernard and J. A. Maruhn; NUcl. Phys. A595 (1995) 346.

[48] A. Dumitru et al.; Phys. Rev. C51 (1995) 2166.

[49] J. Sollfrank, P. Huovinen, M. Kataja, P.V. Ruuskanen, M. Prakash and R. Venugopalan; nucl-th 9607029.

Chapter 2

Application of Hydrodynamical Model to Heavy Ion Collisions:
Limitations and Challenges

The subject of this chapter is to show how the necessity to thoroughly test the hydrodynamical approach and the development of experimental conditions motivated the improvement of the first version of hydrodynamical model and creation of HYLANDER-PLUS.

I will present a general overview about heavy ion collisions experiments at high energies in Section 1. A summary about the use of the hydrodynamical model to interpret the data and the main points to study are presented in Section 2. The limits of the first model and the aspects to improve are discussed in Section 3.

1 Experimental Status

One very important characteristic of a strongly interacting system is the high particle multiplicity. Several hundred (or even thousand) particles are emitted after a collision between two heavy nuclei at 2 or more $GeV/nucleon$. These particles are hadrons, leptons and photons[1].

The phase of the matter between the moment of the collision until the observables particles are emitted can be of four types: a quark gluon plasma (QGP); a hadronic phase; an excited not thermalized hadron matter or an excited not thermalized quark-matter [2]. The careful study of the data helps us to unravel the complex dynamics of high energy nucleus-nucleus reactions.

An experiment in BEVELAC with beam energies of $1-2\ Gev/Nucleon$ showed that energy densities with values three or four times the normal nuclear density can be reached [1]. The possibility to produce matter with even higher values for densities and temperatures, in order to create the physical conditions necessary to check the predictions of QCD, motivated the realization of experimental programs with heavy ions, such

[1] The Appendix 1 gives some definitions necessary to follow the experimental results and their analysis.

[2] The process containing the first two phases can be simulated by a hydrodynamical model.

as those at AGS (Alternating Gradient Synchroton) and SPS (Super Proton Synchroton - CERN). The collisions in such experiments involve beams from *proton* sizes until *lead* sizes and beam energies from 2 to 450 $Gev/nucleon$ on different targets.

In this section I want to give an overview of the most important realized experiments, presenting a summary of information from [2].

1. The large heavy ion experiments at the SPS:

experiment	beams	beam energy	targets	status
NA34-3	S, p	200 GeV/N	W	r.c. 1990
NA35	S, O, d, p	200 GeV/N	C,S,Cu,Ag,Au	r.c. 1992
NA36	S, p	200 GeV/N	S,Fe,Cu,Ag,Pb	r.c. 1990
NA38	S, O, d, p	200 GeV/N	U,W,Cu,Al,C	r.c. 1992
NA44	p, S, Pb	$450, 200, 160$ GeV/N	Be,S,Ag,Pb	r.c. 1996
NA45	p, S, Pb	$450, 200, 160$ GeV/N	be,Au,Pt	running
NA49	p, Pb	160 GeV/N	light, Pb	running
NA50	Pb	160 GeV/N	Pb	running
NA52	Pb	160 GeV/N	Pb	u.c.
NA53	Pb	160 GeV/N	Co,Au	running
WA80	$S; p, O$	$200; 200, 60$ GeV/N	C,Al,S,Cu,Ag,Au	r.c. 1990
WA98	Pb, p	160,200 GeV/N	Pb	u.c.

u.c.: under construction.
r.c.: run completed [3].

The NA34-3, NA38 and NA50 experiments have as physical goals investigation on the dimuon and vector mesons production. NA45 and NA53 experiments work on electron-pair/photon production and electromagnetic dissociation, respectively. Photon production measurements is also the aim of WA80 and WA98 collaboration.

NA35 take measurements involving protons, π^- and K^-. NA36 measures strange baryons (Λ, $\bar{\Lambda}$, Ξ^- and $\bar{\Xi}^+$). NA44 studies Bose-Einstein correlations for protons, pions and kaons. NA49 investigates p, $\bar{p}$, $\pi^\pm$, $K^\pm$ and neutral strange particles (ϕ, K^0, Λ, $\bar{\Lambda}$) production.

The last four experiments mentioned above are of special interest, because they investigate baryons and mesons with high multiplicity and

[3] From WA generation there are 4 other experiments: WA85, WA93, WA94 and WA97. The WA97 is under construction and the others have their run completed. I describe WA80 and WA98 here because comments on them will appear in Chapter 6.

heavy particles involved in the creation of such baryons and mesons. The analysis of these results are essential for a general description of multiparticle production process and will be used in the next chapters.

2. The large heavy ion experiments at the Brookhaven-AGS:

experiment	beams	beam energy	targets	status
E802	Si, O, p	14.5 GeV/N	Al,Cu,Ag,Au	r.c. 1989
E814	Si, O, p	14.5 GeV/N	Al,Cu,Sn,Pb	r.c. 1992
E858	Si	14.7 GeV/N	Al,Cu,Au	r.c. 1995
E859	Si	14.5 GeV/N	Al,Cu,Ag,Au	r.c. 1992
E864	Au	14.5 GeV/N	Al,Cu,Pb	running
E866	Au	11.5 GeV/N	Al,Cu,Ag,Au	approved
E877	Au	11.4 GeV/N	Al,Cu,Au,U	r.c. 1996
E878	Au, Si, p	$14.5, 14.7, 24$ GeV/N	Al,Cu,Au	r.c. 1995
E895	Au	$2-10$ GeV/N	Al,Cu,H	approved
E896	p, Au	$30, 11.6$ GeV/N	Au	u. c.

u.c.: under construction.
r.c.: run completed.

The experiments E858 and E878 investigate anti-deuteron and rare particles production. E864 measures strangelets production.

The experiments in which we are especially interested at this energy range are: E814/E877, which study the low p_t range in pions and kaons spectra; and E802/866, which present data on p, $\pi^{\pm}$ and $K^{\pm}$ production.

To summarize:

Taking into account the size of beam and target in each reaction[4] high energy experiments with heavy ions can be classified into two types: symmetric, when both beam and target nuclei have the same size; or asymmetric, when beam and target sizes are different.

Another important classification is concerning the energy of the collision. Following the tables, one can specify two energy ranges: 'SPS' and 'AGS'. The type of collision and the energy range determine the initial conditions of the simulation (amount of stopping/ transparence effects).

The data can provide information about symmetrical and asymmetrical collisions at SPS and AGS energy ranges.

[4] In this study one is interested in collisions with impact parameter equal zero.

The experimental detection conditions have been improved and new aspects can be investigated as positive hadron, heavy baryon and photon spectra. NA44, E802 and E866 collaborations presented data on p, π^-, K^- [5] and also on π^+ and K^+. E810 presented data on Ξ^-/Λ and other heavy baryons analysis are in preparation. Measurements on photon production have been published by WA80 collaboration.

2 The Hydrodynamical Model and Data Interpretation

The hydrodynamical approach presented here is constructed on two main assumptions [6]: The system is (locally) thermalized and reaches (local) chemical equilibrium [7]. Based on this one can apply the hydrodynamical equations to describe the nuclear fluid under investigation.

The quality of this description also depends on the precision to solve the relativistic equations in a realistic scenario. The scenario of the high energy nucleus-nucleus collision is supposed to have cylindrical symmetry (3 dimensional) and be expanding (time). This picture should be particularly valid for collisions with impact parameter equal zero.

Consequently, the (3+1) dimensional approach using exact numerical solution for the relativistic hydrodynamical equations should offer a 'solid basis' to provide a general description of the process.

To solve the hydrodynamical equations one has to choose two ingredients: 1) the **initial conditions** of the scenario when the hydrodynamical approach starts to be valid and 2) the **equation of state** to describe how it will develop.

A comprehensive study and analysis of the available data in a hydrodynamic approach needs to address, among other things, the following general questions:
1. For a given nuclear collision, what is the degree of stopping or what is the amount of energy available for thermalization ?
2. Are the data consistent with the assumption of local thermal and chemical equilibration ?
3. Are the data consistent with the presence of a QGP in the early stages of the collision ?
4.Are the signatures of a phase transition to be observed in the data ?

[5] Data on negative meson and proton production was previously presented by NA35, NA36, NA49 collaborations.

[6] The physical criterions to use the hydrodynamical model were presented in Chapter 1.

[7] The expression 'local' is used to refer to the application of the concepts thermalization and chemical equilibration to each fluid cell.

All these points can only be checked by comparing calculated results with experimental data.

The presence of a phase transition from quark gluon plasma to hadronic phase could change the whole development of the fireball and influence all final results [8]. The hydrodynamical approach investigates this by introducing (or not) a phase transition in the equation of state and by comparing calculated spectra with data, considering formation of resonances and their decay. In fact, any variant of equation of state can be investigated.

Based on a code containing the described characteristics, the limitation of this analysis and the corresponding conclusions are mainly determined by the number of free parameters in the simulation coming from the initial conditions and from the equation of state.

3 The Limitations of the First Version and the Aspects to Improve

As can be concluded from the last section, a fundamental question for phenomenological models in heavy ion collisions is whether they can describe simultaneously different observables, from different kinds of experiment, in order to check the depth and consistency of its results.

The first version of this model was conceived in 1989 to describe symmetric collisions at SPS energies [9]. The experimental data available for these collisions were from NA35 and NA36 collaboration and consisted in proton, π^- and K^- spectra [10]. The model was restricted to analyze this data (resonance decay was included). In order to describe transparence effects, parameters were introduced to describe the initial conditions of the system (see next chapter).

Despite the fact that these simulations could describe important aspects of the data, these results do not permit a general check of the model and of its assumptions. A general check can be done only by improvement of the aspects mentioned in the last section (regarding the number of free parameters in the simulation) and by application of the

[8] Many works have been published on data interpretation and their connection with the different stages in the development of the fireball formed in the heavy ion collisions, see Appendix 2.

[9] The very first simulation using this code was made for $O + Au$ reactions at SPS energies. The asymmetrical character of the collision was not take into account, the results were obtained by approximation transforming the initial conditions for this reaction to a 'corresponding' symmetric one and using the 1-dimensional full-stopping description from Landau. See for that, for example, ref. [3],[4].

[10] Data on K^0 and Λ production was presented later.

model to describe new experiments (symmetric and asymmetric collisions at SPS and AGS nergies) and new data (positive mesons, heavy baryons and anti- heavy baryons).

The new model containing such improvements and the performance of the new tasks are the subject of the next chapters.

References

[1] R.Stock, Phys. Reports 135 (1986) 259.

[2] Quark Matter 1995, Monterrey-USA, Conference Proceedings, 'A Guide to the high energy heavy ion experiments' - J. Thomas and P. Jacobs.

[3] U. Ornik and R.M. Weiner; Phys.Lett. B263(1991)503.

[4] PhD thesis, "Relativistische Hydrodynamik mit Phaseübergang in der Kosmologie und in Kern-Kern-Stössen", U. Ornik, Marburg Universität, 1990.

Chapter 3
A New Model for New Tasks

Two main conclusions can be drawn so far from the study of heavy ion reactions at AGS (Alternating Gradient Synchroton) and SPS (Super Proton Synchroton - CERN) accelerators:
(i) nuclear matter is not transparent [1]. In particular for collisions of heavy nuclei at AGS ($Au + Au$) the shape of the proton rapidity density distribution around the center-of-mass rapidity suggests an almost total nuclear stopping [2], which also means that high baryon densities are achieved [3].
(ii) The assumption of local thermodynamical equilibrium leads to an astonishing agreement with the data. This follows among other things from the fact that simple fireball models [4],[5] which take into account a longitudinal flow component can explain many features of the data.

These aspects justify the investigation of heavy ion physics with more realistic hydrodynamical models ([6]-[12]).

The basic hydrodynamical model is a generalization of statistical models [13]. It was introduced by Pomeranchuck and Landau [14]-[18], who removed several weak points of the previous fireball models. The unrealistic concept of a fireball in global equilibrium, which is not consistent with the covariant relativistic dynamics of the collision, was replaced by the concept of a system in local equilibrium.

The latter concept is more general and takes into account that the whole system is not yet completely equilibrated, but has inhomogeneities caused by the initial dynamics, which are controled by the strong interaction. It also takes into account that a system at very high temperatures does not only evaporate particles from the surface but also has to expand because of the strong internal pressure. The details of the expansion are determined by the equation of state (EOS), which describes the properties of strongly interacting hot hadronic matter.

The expansion leads to a cooling of the system which changes the absolute particle yields, the chemical composition of the fireball (particle ratios), the momentum distributions, as well as the mean free path, which increases with decreasing density (or temperature) of the system. If the mean free path is large enough the particles decouple (freeze-out) from the fireball.

The concept of local equilibrium and relativistic covariance also requires that decoupling takes place locally, i.e. the particles are emitted

when the fluid cell reaches the decoupling temperature T_f [1]. In other words, below T_f the mean free path becomes too large in order to maintain equilibrium. A local freeze-out usually leads to a very complicated shape of the emission region in space-time (the freeze-out hypersurface).

From the hydrodynamical point of view it is convenient to divide a heavy ion collision into 3 stages:

1. The compression and thermalization of nuclear matter forming the locally equilibrated fireball (*compression stage*).

2. The hydrodynamical expansion of the fireball (*expansion stage*).

3. The decoupling of particles (*freeze-out*).

Supported by the observation of a high amount of stopping, we have extended the (3+1) dimensional hydrodynamical description HYLANDER [19], applied in the past in, e.g. [8], [9],[10] and [12], to the very beginning of the fireball formation process, when the two nuclei touch each other.

The chapter is organized as follows: In Section 1 the formalism of the hydrodynamical model is described. Section 2 presents the options for initial conditions. In Section 3 the equations of state under investigation are introduced. Section 4 shows the improvements in the calculation of observables.

1 The Equations of the Hydrodynamical Model

In their simplest form the hydrodynamical equations do not include dissipative effects. The incorporation of dissipation in a relativistically covariant way is up to now very difficult and requires approximations. Some progress in this field has been made for two and three fluid dynamics and dissipative shock waves [20]-[23]. In the following the discussion will be restricted to one fluid model described by the relativistic Euler equations. Since I consider here central collisions, axial symmetry around the beam direction is assumed.

From the equations of hydrodynamics:

$$\begin{aligned} \partial_\mu T^{\mu\nu} = 0 \quad &, \quad \partial_\mu B^\mu = 0 \\ T^{\mu\nu} = (\epsilon + P)u^\mu u^\nu - P g^{\mu\nu} \quad &, \quad B^\mu = b u^\mu \end{aligned} \tag{1}$$

[1] In this work we choose a critical temperature T_f of the order of the pion mass for the freeze-out criterion.

one obtains:

$$\begin{aligned}
\frac{\partial E}{\partial t} &= -\nabla\left((E+P)\mathbf{v}\right) && \text{energy conservation} \\
\frac{\partial M^i}{\partial t} &= -\nabla(M^i\mathbf{v}) - \frac{\partial P}{\partial x_i} && \text{momentum conservation} \\
\frac{\partial(b\gamma)}{\partial t} &= -\nabla b\mathbf{v} && \text{baryon number conservation} \\
T^{00} = E &= \gamma^2(\varepsilon + Pv^2) \\
T^{0\alpha} = \mathbf{M} &= \gamma^2(\varepsilon + P)\mathbf{v},\ \alpha = 1,2,3
\end{aligned} \tag{2}$$

where $T^{\mu\nu}$ is the energy-momentum tensor, u^μ is the four-velocity, $\mathbf{v}(\vec{x},t)$ is the velocity, P is the pressure, ε is the energy density and b is the baryon density of the fluid. $\gamma = 1/\sqrt{1-v^2}$.

The solution of these equations, which HYLANDER solves in (3+1) dimensions numerically, is determined by the equation of state which can be written in the form

$$P = c^2(\varepsilon, b)\epsilon. \tag{3}$$

It governs the compression, the expansion and the freeze-out surface shape of the fireball.

If the local temperature drops below a critical value (T_f) (corresponding to a critical density $\rho = \rho(T_f)$) the particles are assumed to decouple (locally) from the fluid, i. e. hydrodynamics is not applicable beyond this point. The primordial resulting particle spectra are then given, in the assumption of chemical equilibrium, by the Cooper-Frye formula [24]:

$$E\frac{dN}{d\vec{p}} = \frac{g_i}{(2\pi)^3}\int_\sigma \frac{p_\mu d\sigma^\mu}{exp(\frac{p_\mu u^\mu - \mu_s - \mu_b}{T_f}) \pm 1}, \tag{4}$$

which describes the distribution of particles with degeneration factor g_i and 4-momentum p^μ emitted from a hypersurface element $d\sigma^\mu$ with 4-velocity u^μ [2].

[2] Particles produced with momenta p_μ pointing into the interior of the emitting isotherm ($p_\mu d\sigma^\mu < 0$) were assumed to be absorbed and therefore their contribution to the total particle number was neglected. In ref [25] this effect was indeed estimated to be negligible. Another effect is the interaction of the freeze-out system with the rest of the fluid. This effect can be estimated by comparing the evolution of the fluid with and without the frozen-out part. This is done by equating the frozen-out part with that corresponding in the equation of hydrodynamics to the case $P = 0$. The fluid parameters are modified by this procedure at a level not exceeding 10% [19].

After the cascading of the resonances one obtains the final observable spectra.

For a given EOS the procedure to determine the strangeness and baryonic chemical potentials is based on the requirement that the energy density, baryon density and strangeness density of the fluid are equal to those of the system after chemical freeze-out (see, for details,[8],[19] or [26]).

2 Initial Conditions

2.1 The first version

In the earlier approach (for example, [8, 9, 12]) at SPS energies one took into account that, due to transparency effects, the local equilibrium state is reached after undergoing a non-equilibrium stage, which is not treatable with hydrodynamics. Therefore one started the simulation in an intermediate state which one has to model by introducing five parameters based on "reasonable" assumptions about the initial configuration. However both for $S + S$ and $Pb + Pb$ collisions one found that the inelasticity necessary to describe the data was larger than 70%. For lower energies (AGS) the inelasticity (or amount of stopping) is expected to increase. This parametrized option for the initial conditions will be used in Chapter 5.

2.2 The new version

In the present work the first code was extended to use a different approach to the hydrodynamics of heavy ion collisions suited for processes with (almost) full-stopping.

It is based on the original Landau model [14, 15] where the process of stopping is also treated hydrodynamically, rather than being parametrized by some initial conditions as in [9, 10]. As will be explained below, the present approach constitutes an important improvement over the old Landau approach as it eliminates most approximations he made.

The starting point of the model are two colliding cylinders at zero temperature and nuclear ground state density. The width in longitudinal (beam) direction is given by the Lorentz-contracted nuclear diameter in the equal velocity frame. This problem was solved by Landau analytically [14] with the following approximations:

1. the assumption of 1-dimensional shock waves,

2. the one-dimensional (1-d) hydrodynamical description for the beginning of the expansion process followed by an approximated (3+1) dimensional analytical solution and

3. an equation of state of the type $P = c_0^2 \varepsilon$ where c_0 is the constant velocity of sound.

In the present work none of these approximations will be used, since both the *compression stage* and the *expansion stage* are described by a fully (3+1)-dimensional hydrodynamical simulation [3].

As a consequence one has additional contributions to the particle spectra from the very early *compression stage*. The $Au + Au$ system at AGS spends about 4 fm/c in this stage[4].

Given the fact that, due to this treatment, there are no free parameters necessary to describe the initial conditions of the fireball, it becomes now possible to study the sensitivity of the results to the properties of the EOS. This will be done by applying our solutions of (3+1) dimensional hydrodynamics to $Au + Au$ reaction at AGS (Chapter 4). This initial condition option is also used to simulate $S + Au$ reaction at SPS (Chapter 6).

3 The Equations of State

3.1 The first version

With this version one type of EOS was mostly used to solve numerically the relativistic hydrodynamic equations [5].

It is an EOS given by a parametrization of lattice-QCD results [27] and two asymptotic conditions: $\lim_{T\to\infty} c_0^2 = 1/3$ and $\lim_{T\to 0} c_0^2 = 1/7$ [25, 28]. It describes a first order phase transition between quark gluon

[3] Another improvement which the new approach presents is that the starting point in this calculation are two colliding *spheres* Lorentz contracted in the longitudinal direction.

[4] Landau used an $1-d$ approximation of this stage and neglected its contribution to the spectra. This is justified only at extremely high energies where the Lorentz contracted longitudinal diameters before collision are very small compared to the lifetime of the system. It is not the case for AGS energies. Squeeze-out effects and transverse motion are also not present in Landau's approach.

[5] Some simulations were realized with this version using other very simplified EOS without phase transition, as a pion gas EOS. The possibility to carefully investigate the influence of the phases on the particle spectra, opened with the new version using the full-stopping option for the initial conditions, leads to improve this aspect in a realistic way.

plasma and hadronic matter at $T = 200 MeV$ [6]. Although this EOS does not contain baryons, the hydrodynamical equations (1,2) do consider them explicitely. This is not a contradiction, but rather corresponds to the assumption that the presence of baryons does not modify drastically the EOS. The fact that the data can be described with such an EOS gives some support to this assumption [7].

I will refer to this EOS as **lattice-EOS**, it will be used in the simulations presented in Chapter 5 and 6.

3.2 The new version

In Chapter 4 two models for the EOS will be investigated as an input to solve numerically the relativistic hydrodynamic equations with the HYLANDER-PLUS code: the just above presented one (lattice-EOS) and a **resonance gas EOS**.

Two versions of a resonance gas equation of state [20, 30], which differ in the number of included resonances, are considered. In the following I will refer to **RG1.5** for a resonance gas including resonances with masses up to 1.5 GeV and **RG2** for a gas of resonances of masses up to 2 GeV. In these EOS, in opposition to the lattice-EOS, the baryon chemical potential is considered explicitly.

4 Calculation of Observables

4.1 The first version

A table with the analyzed particle spectra is presented. The collaborations, which published the data described by the model, are mentioned:

	p	π^-	K^-
S+S	NA35	NA35	NA35
Pb+Pb	NA49	NA49	NA49

4.2 The new version

The new version takes into account new aspects of the data, discussed in the last chapter. I present a general view of particle spectra analyzed with the new model:

[6] In [27] a pure gluonic system is considered. Results considering dynamical quarks lead to a critical temperature T_c between 150 and $220 MeV$ [29] (cf also Quark Matter 96).

[7] Lattice QCD calculations with $\mu_b \neq 0$ do not yet exist.

	p	π^-	π^+	K^-	K^+	h.b.	h.a-b.	phot.
S+S	NA35	NA44	NA44	np	np	np	np	ny
Pb+Pb	NA49	NA44	NA44	np	np	np	np	[31]
Au+Au	E802/866	E866	E866	E866	E866	[32]	[32]	[31]
S+Au	ny	ny	ny	ny	ny	ny	ny	WA80

h.b.: heavy baryons
h. a-b.: heavy anti-baryons
phot.: photons
np: not published
Ref.: calculation was published as predictions.
ny: calculations not yet made or not yet completed.

To summarize, the new version, called HYLANDER-PLUS, contains:
a) all possibilities for calculation from the first version,
b)the mentioned extension of (3+1)-dimensional description to the early stages of the collision process,
c)the possibility to use different equations of state to solve the hydrodynamical equations and obtain the particle spectra,
d)the calculation of positive (and negative) hadronic spectra,
e)the calculation of spectra for heavy-baryons, anti-baryons and electromagnetic probes.

References

[1] see for example: J. Stachel and P. Braun-Munzinger, Phys. Lett. B 216(1989)1; E814/E877 Collaboration, Phys. Rev. Lett. 70(1993)2996.

[2] BNL-AGS E802/866 Collaboration, Nucl.Phys. A590 (1995) 519c.

[3] L. Ahle et al., E866 Collaboration, Nucl.Phys. A590 (1995) 249c.

[4] E. Schnedermann, J. Sollfrank and U. Heinz, Phys. Rev. C48(1993)2462.

[5] P. Braun-Munzinger, J. Stachel, J.P. Wessels and N.Xu, Phys. Lett. B344(1995)43.

[6] R.B. Clare and D. Strottman, Phys.Reports 141(1986)177.

[7] R. Waldhauser, D.H. Rischke, U. Katsher, J.A. Maruhn, H. Stoecker and W. Greiner; Z. Phys. C54(1992)459.

[8] U. Ornik and R.M. Weiner; Phys.Lett. B263(1991)503.

[9] J. Bolz, U. Ornik, R.M. Weiner; Phys.Rev.C 46(1992)2047.

[10] J. Bolz, U. Ornik, M. Plümer, B.R. Schlei and R.M. Weiner; Phys.Lett B300(1993)404; Phys.Rev. D47(1993)3860.

[11] for a recent review see D. Strottman, Nucl. Phys. A566(1994)245c.

[12] U. Ornik, M. Plümer,B.R. Schlei,D. Strottman,R.M. Weiner; Phys. Lett. B376(1996)212; Phys. Rev. C 54 (1996) 1381.

[13] E. Fermi, Prog. Th. Phys. vol.5(1950)570; Phys. Rev. 81 (1951)683.

[14] L.D. Landau; Izv. Akad. Nauk.(USRR) 17(1953)51.

[15] Collected Papers of Landau; Pergamon Press, London (1965), paper number 88.

[16] I.Y. Pomeranchuck; Dokl.Akad.Nauk.(USRR) 78(1951)889.

[17] S.Z. Belenkij and L.D. Landau; Fiz.Nauk. 56(1955)309.

[18] S.Z. Belenkij and G.A. Milekin; Zh.Eksp.Theor.Fiz. 29 (1955)20; Sov.Phys.-JEPP 2(1976)14.

[19] PhD thesis, "Relativistische Hydrodynamik mit Phaseübergang in der Kosmologie und in Kern-Kern-Stössen", U. Ornik, Marburg Universität, 1990. U. Ornik and R.M. Weiner; Phys. Lett. B263(1991)503.

[20] L. Mornas and U. Ornik, Nucl. Phys. A587(1995)828.

[21] P. Danielewicz, Phys.Lett. B 146(1984)168.

[22] M.S. Ganagi and A.V. Gopalakrishna, Astrophys. Spa. Sci. 129(1987)281.

[23] M.P. Galipo, Lett. Nuov. Cim. 38(1983)233,427,544.

[24] F. Cooper,G. Frye and E. Schonberg; Phys.Rev.D 11(1975)192.

[25] U. Ornik, F.W. Pottag, R.M. Weiner; Phys. Rev. Lett. 63(1989) 2641.

[26] U. Ornik, M.Plümer and D. Strottman; Phys.Lett. B314(1993)401.

[27] K. Redlich and H. Satz, Phys. Rev. D33(1986)3747.

[28] U. Ornik and R.M. Weiner; Phys.Rev. D36(1987)1263.

[29] T. Blum, T. DeGrand, C. DeTar, S. Gottlieb, A. Hasenfratz, L. Kärkkäinen, D. Toussaint and R.L. Sugar; Phys. Rev. D50 (1994) 3377 and references therein.

[30] R. Hagedorn; Nuov. Cim. Suppl. 3(1965)147. J. Rafelski and R. Hagedorn; in Statistical Mechanics of Quarks and Hadrons, Bielefeld Symposium (1980), ed. H. Satz (North-Holland, Amsterdam, 1981), pg.253.

[31] N. Arbex,U. Ornik, M. Plümer, A. Timmermann and R.M. Weiner.; Phys. Lett. B345(1995) 307.

[32] N. Arbex, U. Ornik, M. Plümer and R. M. Weiner, Phys. Rev. C55 (1997) 860.

Chapter 4

Probing the equation of state in $Au + Au$ at 11 $GeV/nucleon$

The effect of (i) the phase transition between a quark gluon plasma (QGP) and a hadron gas and (ii) the number of resonance degrees of freedom in the hadronic phase on the single inclusive distributions of 16 different types of produced hadrons for $Au + Au$ collisions at the Brookhaven Alternating Gradient Synchroton (AGS) energies is studied.

I have used the option *without free parameters* for the initial condition, to be applied in simulation of collisions with very high amount of stopping, as presented in the last chapter.

Two different equations of state (EOS) are used - one describing a phase transition from QGP to the Hadronic Phase and two versions of a purely hadronic EOS. The influence of the presence of quark gluon plama on particle production can be investigated.

Section 1 contains the results, divided in two topics: 1.1 Energy density, baryon density and lifetime and 1.2 Particle spectra. Reproduction and analysis of measured meson and proton spectra are presented, as well as predictions for anti-protons, deltas, anti-deltas and hyperons. The sensitivity of various production channels to the EOS is also analyzed.

In section 2 three remarkable results from the simulations are discussed: a) the low m_t enhancement in π^- spectra, b) the ratio N_{Ξ^-}/n_Λ and c) the rate K/π. Section 3 contains a discussion about the results[1].

1 Results

1.1 Energy density, baryon density and lifetime

Table 1 shows the values for maximum energy density, maximum baryon density and the time it takes until the fireball is completely transformed into free particles (lifetime). All these simulations start at the moment of the impact between the nuclei ($t = 0$).

[1]The results presented in this chapter have been published in Phys. Rev. C55 (1997) 860.

The system spends about one third of its lifetime in the compression stage, confirming the importance of this part of the process, neglected in the classical Landau approach.

The values for lifetime, maximum baryon and energy density for lattice-EOS and RG2 are surprinsingly similar, but this does not necessarily mean that the behaviour of each fluid cell (and of the whole fluid) until freeze-out is also the same. To investigate this I study the trajectory of the fluid elements in a phase diagram of energy density versus temperature, for the three EOS (see Fig.1). In this figure the temperature and energy density for each fluid cell with $T > 139\ MeV$ (which means for all $\vec{x}$ and t) is plotted, starting at the beginning of the simulation.

Table 1

	lattice EOS	RG2	RG1.5
max. energy density	6.6 GeV/fm^3	7.5 GeV/fm^3	2.5 GeV/fm^3
max. baryon density	13.6 n_0	16.7 n_0	5.6 n_0
lifetime	10 fm/c	10 fm/c	15 fm/c

Maximum values for energy density, baryon density and lifetime for hydrodynamical simulations (HYLANDER-PLUS) using three different EOS. n_0 is the normal baryon density.

One can see that for lattice and RG2 the fluid elements describe a trajectory in almost the same energy density and temperature range. For both simulations the fluid elements can reach temperatures up to 215 MeV and energy densities bigger than 6 GeV/fm^3, for lattice-EOS this correspond to temperatures slightly above the phase transition temperature.

The trajectory for RG1.5 is located in a very different range. The explicit dependence on a baryonic chemical potential in RG2 and RG1.5 appears just in the "width" of the curve. It is interesting to note that even in the case of RG1.5 and RG2 where μ enters explicitly in the calculation the baryon dependence is weak, i.e. the "width" of these curves is surprisingly small.

The similarity in the results for energy density, baryon density and lifetime for lattice-EOS and RG2 can be explained by Hagedorn's model [1]. Increasing the number of resonances in the hadronic gas EOS induces a phase transition-like behavior in the development of the fireball[2].

[2] An important and obvious question is whether this behaviour of the fluid elements

FIGURE 1

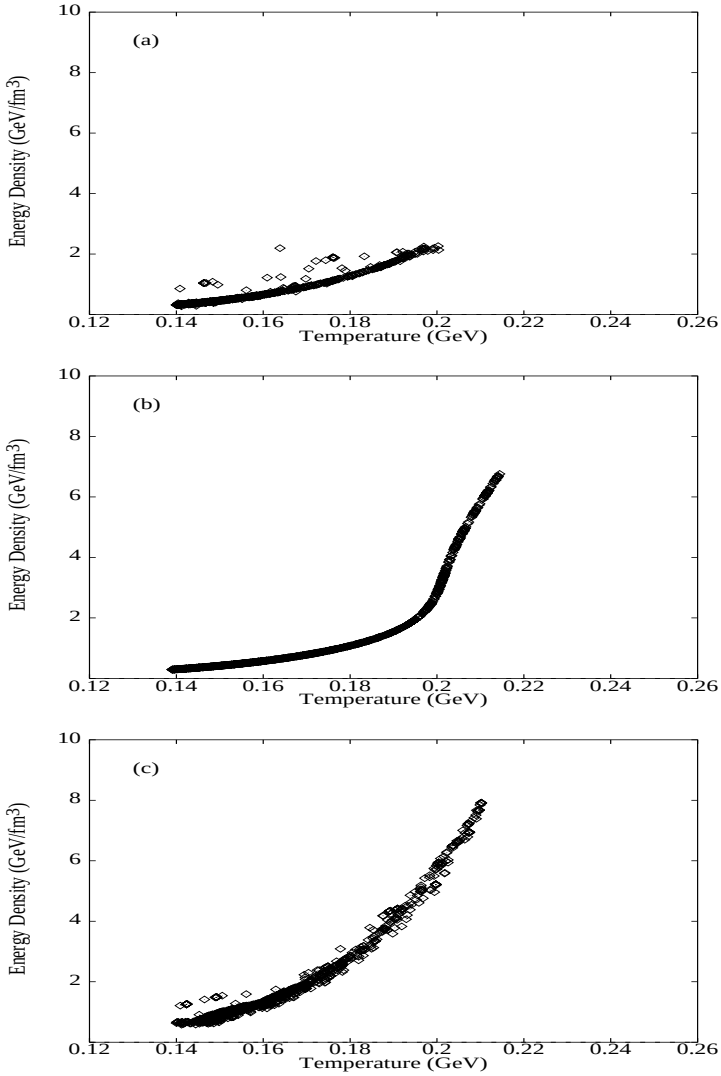

Fig. 1: Plot of temperature and energy density of each fluid cell with T > 139 GeV, from the beginning of the collision, for the hydrodynamical simulation (HYLANDER-PLUS) using the different EOS. The figure shows the trajectory of the cells in the (ϵ, T) diagram until they freeze out. a) for RG1.5, b) for lattice-EOS and c) for RG2.

---

will be the same for other nuclear reactions. I performed a simulation for $Pb + Pb$ at 160 $GeV/nucleon$ to try to answer this question. I used the same initial condition as in this chapter and two EOS, namely lattice and RG2. The resulting trajectory of the fluid elements differs from that for the AGS system. The difference between both EOS appears for temperatures larger then 0.2 GeV. What this implies for the particle spectra will be discussed elsewhere [2].

The sensitivity of the produced particle spectra to these differences in the EOS [3] is the subject of the following subsections.

1.2 Particle spectra

At freeze-out temperature one treats explicitly the emission of protons, neutrons, pions, kaons, anti-protons (directly produced), the particles/resonances: $\omega(783)$,η,$\eta\prime$, ρ,K_0,K^*, Δ,Σ,Λ,Ξ and corresponding anti-particles (see [3]). The results I present in the next subsection take into account the contribution from the decay of particles.

1.2.1 Spectra of protons, pions and kaons

In Figure 2 the transverse mass ($m_t = \sqrt{m^2 + p_t^2}$) spectra of protons, positive and negative pions for different rapidity intervals from our **RG1.5** simulation with experimental data [4, 5] are compared. All spectra obtained for this EOS differ considerably from the data.

Figure 3 shows the corresponding results from the simulation using the **lattice-EOS**. One can see that, except for the very central region (last curve), where the proton production is overestimated, the experimental proton spectra are very well fitted. The fits for positive and negative pions show the same tendency: significant deviation from the data is observed only in the very central rapidity region (first curve). In all cases there is a small overestimate of particle production at large p_t, which means in hydrodynamical terms an overprediction of transverse flow.

In the last section I mentioned the similarity in the lifetime, baryon and energy density, as well as the trajectory of the fluid elements arising from lattice-EOS and RG2 simulations. Therefore one expects that the RG2 spectra are more similar to the spectra obtained using lattice-EOS than to the ones using RG1.5.

The simulation using RG2 confirmed this expectation. One can see this in Figure 4 where I consider the m_t spectra resulting from the simulation with **RG2**. Particularly for pions one observes a very good agreement with the data. Even the overestimate of pions at large p_t observed for the lattice-EOS simulation vanishes. In the case of protons we observe deviations only in the very central rapidity region.

[3] By imposing energy-momentum conservation at freeze-out we reduce the errors involved by the fact that the Cooper-Frye formula assumes an ideal gas EOS, while the fireball is governed by the RG1.5 or RG2 EOS, to a level of about 5%. For the lattice-EOS this problem does not exist because of the asymptotic condition.

FIGURE 2

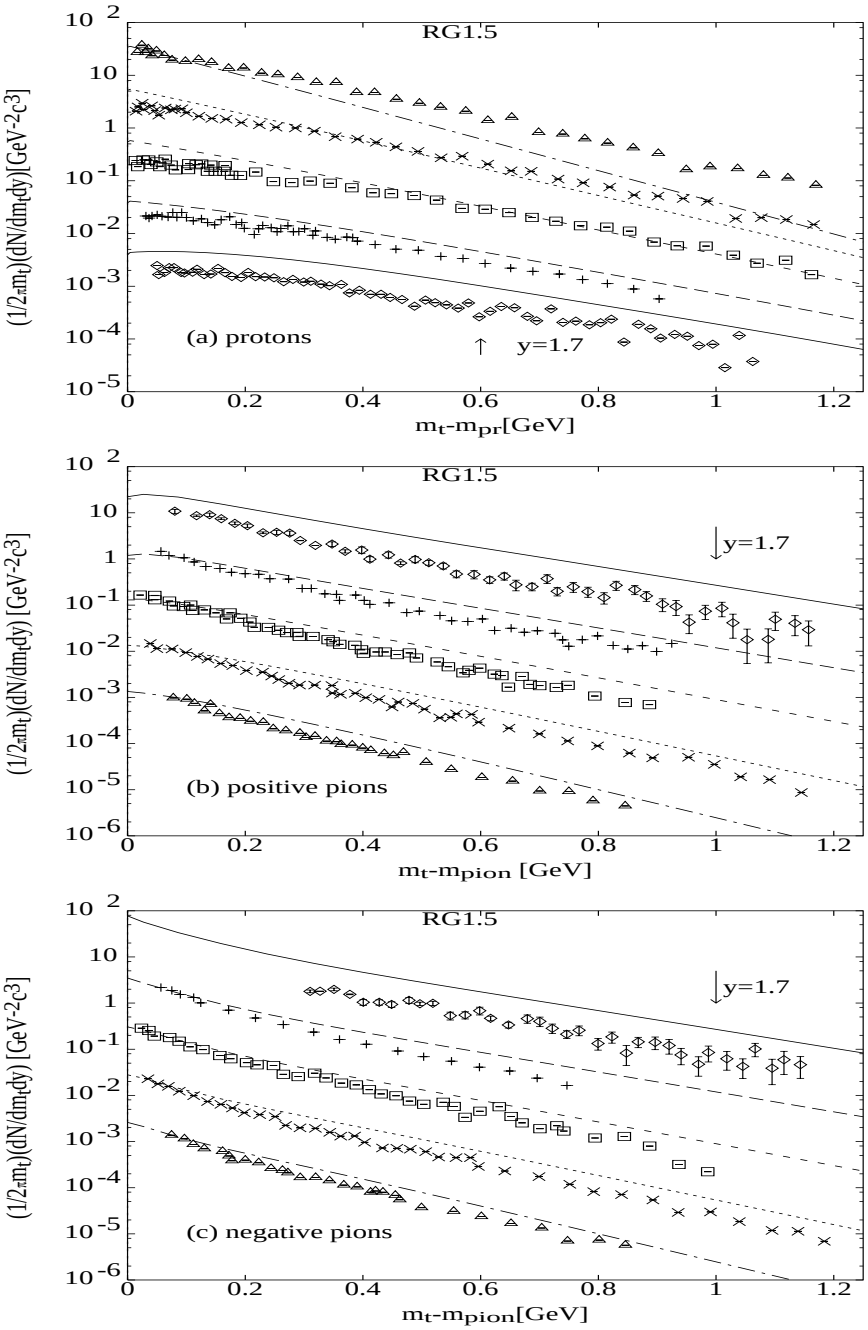

Fig. 2: Transverse mass spectra for five rapidity intervals for protons, positive and negative pions using the equation of state RG1.5. The data (taken from [5] [4]) and hydrodynamical simulated curves (HYLANDER-PLUS) are shown for rapidity bins from 1.7 to 2.5 (for pions), from 0.9 to 1.7 (for protons). In both cases the bin size is 0.2 and the bins are centred around $y_{central} = 1.6$.

FIGURE 3

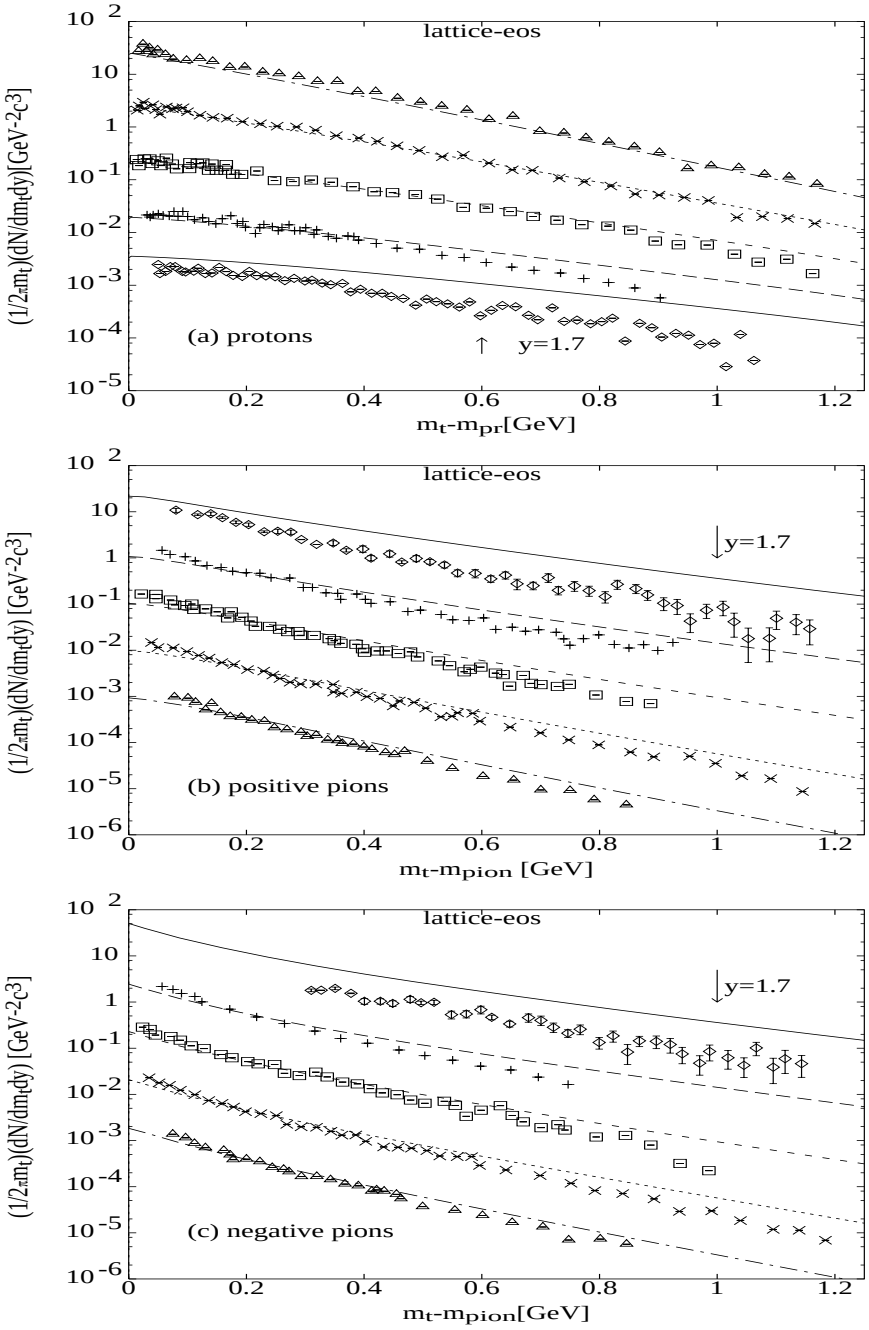

Fig. 3: Transverse mass spectra for five rapidity intervals for protons, positive and negative pions using lattice EOS. The data and rapidity intervals are the same as in Fig. 2.

FIGURE 4

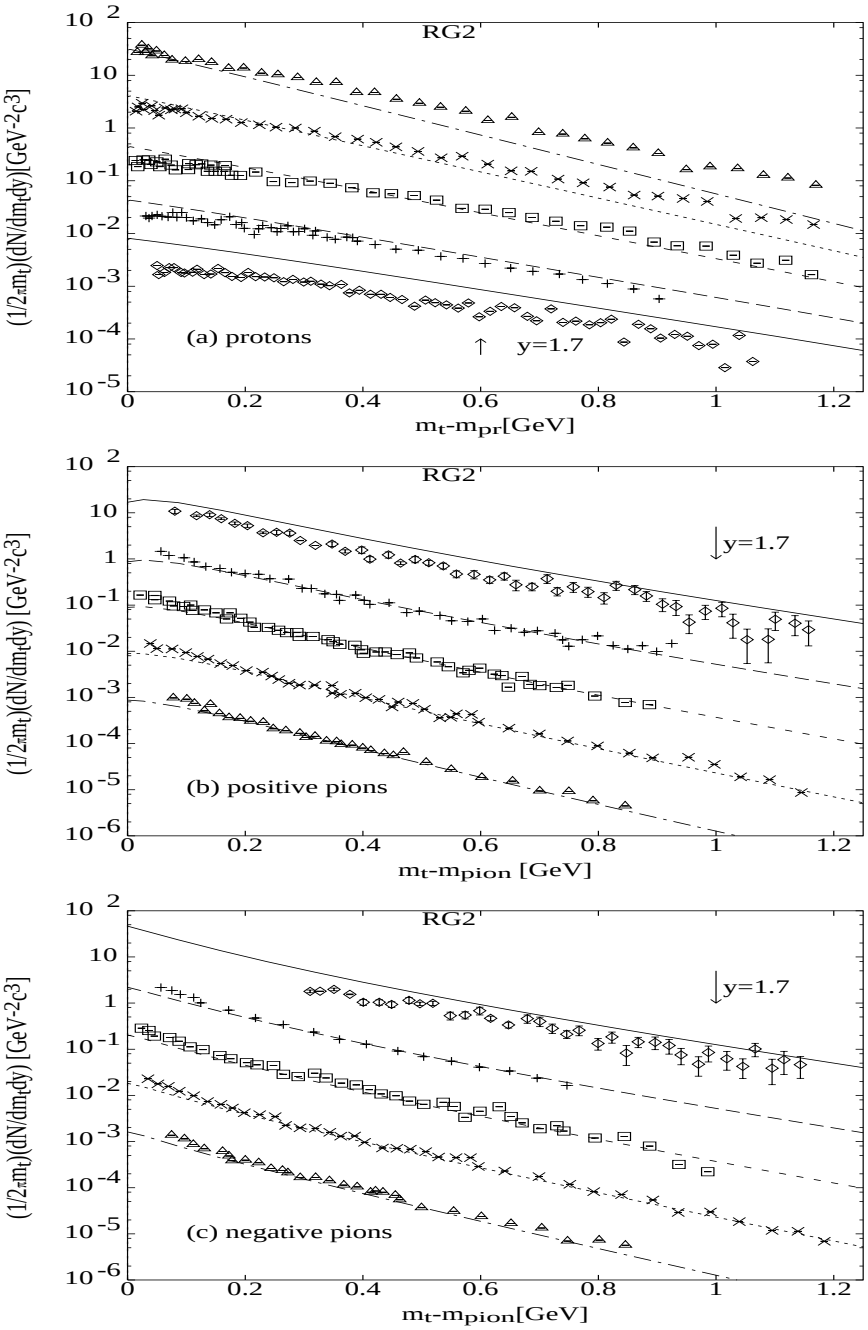

Fig. 4: Transverse mass spectra for five rapidity intervals for protons, positive and negative pions using RG2. The rapidity intervals and data are the same as in Fig. 2 and 3.

FIGURE 5

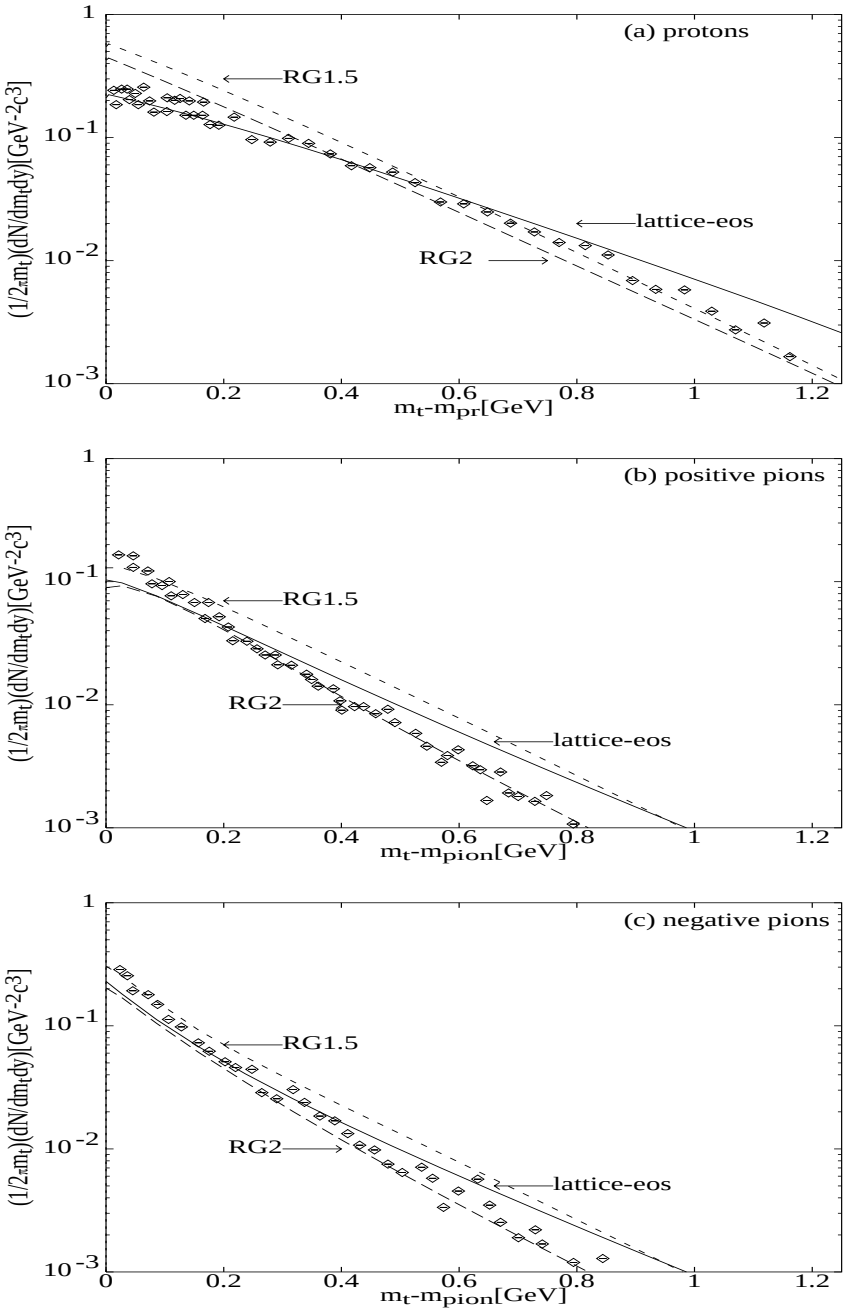

Fig. 5: Comparison of the m_t spectra at fixed rapidity ($y = 2.1$ for pions and $y = 1.3$ for protons) for hydrodynamical simulations (HYLANDER-PLUS) using lattice, RG2 and RG1.5 equations of state.

In Figure 5 the spectra, at fixed rapidity, for all three simulations are compared. Here one can see that for the protons the best fit is clearly given by the lattice-EOS simulation. For positive pions the simulation by RG2 is better and for negative pions the best results are obtained with both lattice-EOS and RG2.

If one takes into account the so far available data one can already conclude that a medium with a large number of internal degrees of freedom (a very "soft" EOS) is favoured.

All three simulations show at midrapidity an overestimate of proton and pion yields. I attribute this effect to the transverse squeeze-out of nuclear matter which has its maximum at zero impact parameter (central collisions). I recall that the data are sampled over a finite impact parameter (b) region [4] , whereas the simulation is really at $b = 0$, therefore the squeeze-out appears diluted in the data.

However I do not encounter the problem cited in [4] (and references quoted there for Monte Carlo models) which could not reproduce the flatness and shape of the proton and pion spectra.

The enhancement at low m_t exhibited in the π^- spectra is present in all three simulations. One can reproduce this effect in a natural way just by taking into account resonances, baryon conservation and strangeness equilibration [5]. This manifests itself not only as a change in the shape of the π^- spectra but also as an increase of the total multiplicity of negative pions compared to the positive ones. A more precise analysis of π^- and π^+ production will be presented in section 2 and Chapter 5.

Now we turn to rapidity distributions [6] (Fig. 6).

For protons and pions the already observed tendency is confirmed, namely the results arising from the simulations with lattice-EOS and RG2 are closer to the data than RG1.5.

In pion production one can see here explicitly that the hydrodynamical simulation produces more negative pions than positive ones, a fact which is confirmed by the experiment.

In the rapidity distribution analysis I include a comparison between the results and strange particle production data. This is of particular importance because of the well known proposal to look at strangeness production as a signature of QGP (cf. e.g. [6] - [9] for more recent references).

[4] The "very central" data (4% centrality) for $Au + Au$ AGS correspond to an impact parameter $b < 2.6$ fm (Y.Akiba, private communication and QM96).

[5] In [5] statistical and systematic errors in the data was invoked to partially explain the observed enhancement.

[6] The calculation of rapidity distributions from the model do not contain the phase space cuts at low m_t.

In Figure 6 one also can see that for the kaon rapidity spectra the difference between the three simulations is more pronounced, particularly for negative kaons. The comparison with preliminary data favours the lattice-EOS.

FIGURE 6

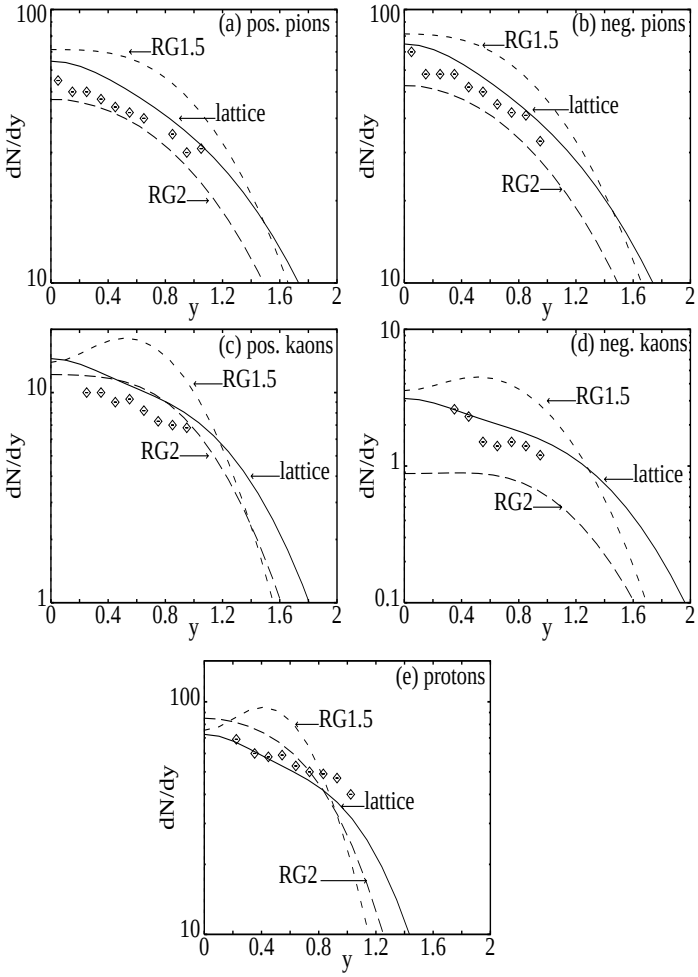

Fig. 6: Rapidity distribution for protons, pions and kaons for hydrodynamical simulations (HYLANDER-PLUS) using lattice, RG2 and RG1.5. equations of state. The data are from [5].

As an preliminary conclusion for this subsection one can say that the results are generally in surprisingly good agreement with the data, especially if one takes into account that I do not use any parameters other than those that enter the EOS.

One can also conclude that presence or absence of a phase transition can not be determined by the analysis of m_t spectra of protons and

pions. The situation appears to be different if one looks at other aspects such as the total number of produced protons and pions (see Table 2) and the rapidity distributions of protons, pions and especially kaons, where one observes remarkable differences between the spectra resulting from the three simulations.

Since kaon production in a baryon-rich medium is linked to hyperon production and chemical equilibration one expects from those also a sensitivity in the hyperon yield related to the EOS. Motivated by this fact I will investigate in the following the rapidity distributions of deltas, hyperons and their corresponding anti-particles. I also consider anti-proton production.

The data are generally better described if one uses a "softer" EOS. Because of that from now on I will restrict the discussion to the results from the simulations with the lattice-EOS and RG2.

1.2.2 Predictions for anti-baryon and heavy baryon production

In Figures 7,8 and 9 the rapidity distributions for anti-protons, heavy baryon and heavy anti-baryon production are shown. Table 2 shows the total particle number for all created particles and anti-particles for the three simulations.

FIGURE 7

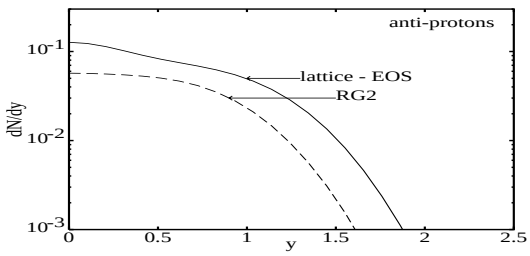

Fig. 7: Rapidity distribution for anti-protons for hydrodynamical simulations (HYLANDER-PLUS) using lattice and RG2.

The lattice-EOS produces a larger or a comparable number of heavy baryons and heavy anti-baryons than RG2 (except for Δ). The largest differences are predicted for Ξ, Ω, $\bar{\Delta}$ and $\bar{p}$ [7].

For heavy baryons (Fig. 8) differences appear in the forward rapidity spectra ($y > 1.0$). The Ω production differs in the whole rapidity range.

[7] The direct $\bar{p}$ production contributes with only $\sim 30\%$ to the total $\bar{p}$ abundancy total numbers.

FIGURE 8

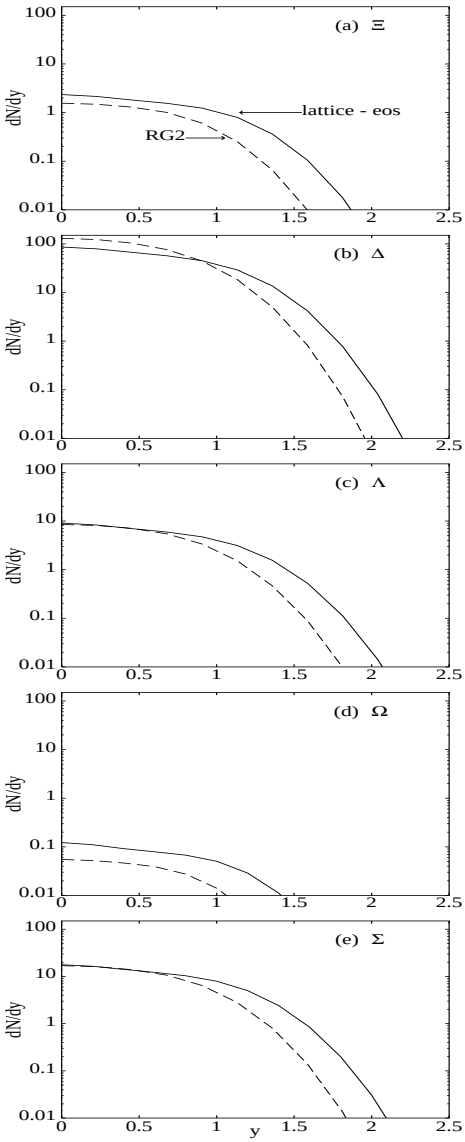

FIGURE 9

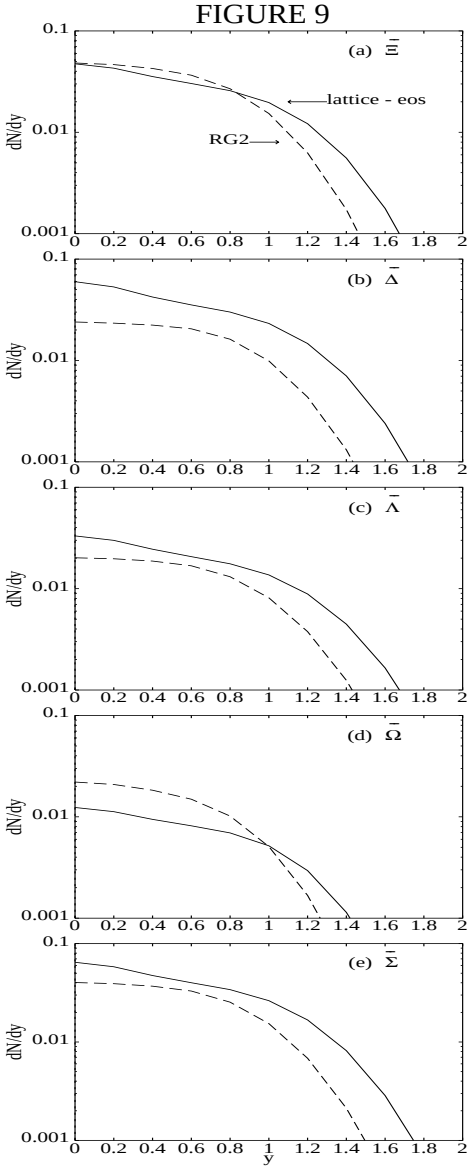

Fig. 8: Rapidity distribution for heavy baryon production ($\Delta, \Sigma, \Lambda, \Omega$ and Ξ) for hydrodynamical simulations (HYLANDER-PLUS) using lattice EOS and RG2.

Fig. 9: Rapidity distribution for heavy anti-baryons production ($\bar{\Delta}, \bar{\Sigma}, \bar{\Lambda}, \bar{\Omega}$ and $\bar{\Xi}$) for hydrodynamical simulations (HYLANDER) using lattice EOS and RG2.

For the heavy anti-baryons rapidity spectra (Fig.9) differences appear in the whole rapidity range, except for $\bar{\Xi}$, where the difference appears only in the forward region ($y > 1.0$).

Table 2

particle	lattice EOS	RG2	deg. factor	data
p	132.800	140.200	1	160
π^+	140.200	100.800	1	115
π^-	155.000	109.000	1	160
K^+	29.000	25.800	1	-
K^-	6.000	2.000	1	-
Ξ	4.100	2.400	2	-
Δ	153.300	197.600	4	-
Λ	16.200	13.700	1	-
Ω	0.200	0.080	1	-
Σ	31.300	26.800	3	-
$\bar{p}$	0.200	0.100	1	-
$\bar{\Xi}$	0.075	0.080	2	-
$\bar{\Delta}$	0.095	0.044	4	-
$\bar{\Lambda}$	0.055	0.036	1	-
$\bar{\Omega}$	0.020	0.030	1	-
$\bar{\Sigma}$	0.100	0.070	3	-

Table 2: Total multiplicities of produced particles and anti-particles from simulations using the two different EOS. The numbers take into account the shown isospin degeneracy factors. The data are from [5] (The error bars are around 10%. Y.Akiba, private communication).

2 Highlights

In the following I would like to emphasize three remarkable results of the calculations: (a) the enhanced π^- production compared with π^+ production; (b) the ratio N_{Ξ^-}/N_Λ; and c) the rate K/π.

a) Taking into account baryon and strangeness conservation as well as strangeness equilibration at AGS energies and including the decay of the resonances in the final stage in the model the difference $N_{\pi^-} - N_{\pi^+}$ is given by:

$N_{\pi^-} - N_{\pi^+} \simeq$
$0.64N_\Lambda + N_{\Sigma^-(1190)} + 0.64N_{\Sigma^0} - 0.48N_{\Sigma^+} + 1.64N_{\Xi^-} + 0.64N_{\Xi^0}$,
i.e., the hyperons and their decay mainly determine the difference between π^- and π^+ total numbers. Since the model fits both the π^- and π^+ spectra, one has a natural and simple explanation for the experimentally observed difference in the multiplicities of positive and negative pions.

This also explains the experimental observation from flow analysis that π^- flow is correlated with the protons [8], as the π^- contribution from hyperon decays is connected to the baryon flow. More results on this subject will be presented in the next chapter.

b) In [10] multi-strange hyperons ($S \geq 2$) and strangelets are suggested as better signatures than single-strange particles ($S = 1$). The first report about Ξ^- production in heavy ion collisions at AGS [11] (for $Si+Pb$) mentions that the observed rates are at least 5 time bigger than all present cascade model predictions. There are no such data available for $Au + Au$ collisions at AGS energies at the moment, but $Si + Pb$ at AGS energies constitutes an experiment in the same energy range, with a high baryon density and a high amount of stopping. Encouraged by these aspects I compare the obtained results with these data.

For $Au + Au$ I find the following results:

$N_{\Xi^-}/N_\Lambda = 0.126$ (lattice-EOS)

$N_{\Xi^-}/N_\Lambda = 0.090$ (RG2)

which are compatible with the experimental value of 0.12 ± 0.02 for $Si + Pb(AGS)$. However the difference between lattice-EOS and RG2 simulations is not very big which leads to the tentative conclusion that the Ξ^- production does not necessarily serve as a better signal for QGP than other strange particle yields. These ratios could be analized as signal for chemical equilibration.

c) The experimental ratios K/π for $Si + Au$ (AGS) were measured and published in [12]. The values are $K^+/\pi^+ = 0.192 \pm 0.03$ and $K^-/\pi^- = 0.036 \pm 0.008$ in the mid-rapidity region and they have been presented as intriguing results because of the large strangeness yields compared with $S + S$ (SPS), where both values are about 0.11. For $Au+Au$ (AGS) experiment the ratio K^+/π^+ is found to be 0.21 [5] and the negative ratio was not yet published.

The results are remarkable in the sense that there are no strange particles present in the initial state and a significant rate of strange particle production is only understandable if a strange chemical equilibrium is established during the reaction. Strangeness equilibration however is not easy to justify in a pure hadronic scenario.

From the calculations, which include the assumption of strangeness equilibrium, I find:

$N_{K^+}/N_{\pi^+} = 0.207$ (lattice-EOS) and 0.256 (RG2),

which are in surprisingly good agreement with the experimental results,

[8] T.Hemmick private communication and QM96.

especially for the lattice-EOS scenario. The numbers from the lattice-EOS and RG2 simulation are not very different and we can conclude therefore that this result is a strong indication of local equilibration (including strangeness equilibrium) of the system. The signal however is not very sensitive to the concrete type of the EOS.

On the other side, clear differences appear (see Table 2) for the other ratio: $N_{K^-}/N_{\pi^-} = 0.038$ (lattice-EOS) and 0.018 (RG2). Experimental information about this ratio (not yet published) is very important and should be treated with care.

From the results one can conclude that a hadronic scenario considering strangeness equilibration can also explain the difference between the positive and the negative ratios [9].

3 Discussion

I have demonstrated that the (3+1)-d hydrodynamical model presented above can describe quite reasonably the AGS data for $Au + Au$ reactions. This suggests that the hypothesis of local thermodynamical equilibrium applies also for the early stage of the reaction.

I showed that both an EOS based on QCD lattice calculations exhibiting a phase transition between quark gluon plasma/hadronic phase (lattice-EOS) and a resonance gas EOS including resonances with masses up to 2 GeV (RG2) have the essential physical properties necessary to describe the measured proton and pion m_t spectra. An EOS described by a resonance gas with a small number of degrees of freedom (RG1.5) is not consistent with these data. However as shown by Hagedorn [1] the RG2 scenario is related to the idea of a phase transition. This phase transition-like behaviour becomes even more pronounced if one adds higher resonances. However, I note that the assumption of strange chemical equilibration, which is assumed to be present even in this hadronic scenario, is not easy to justify in the case of a pure hadronic EOS.

In an analysis including the m_t spectra for protons and pions, the total multiplicities of produced protons and pions and their rapidity distributions one can conclude that the lattice-EOS provides an overall better description of the $Au + Au$ (AGS) experimental data than a hadronic EOS.

I have also calculated the particle spectra for anti-baryons and heavy anti-baryons and the rates π/K and Ξ^-/Λ in order to investigate the influence of a phase transition on the production of these particle species.

[9] Other aspects in this discussion related to $Si + Au$ (AGS) is presented in [13]

Generally the simulation with the equation of state containing a QGP-hadronic phase transition between a hadronic phase and a QGP predicts a larger total multiplicity of heavy baryons and anti-baryons than with resonance gas. The largest differences in the number of produced particles appear for Ξ, Ω, $\bar{p}$ and $\bar{\Delta}$.

In all heavy baryon and heavy anti-baryon rapidity distributions, the strong difference between both EOS scenarios appears in the forward region of rapidity, $y > 1.0$. For Ω and heavy anti-baryons (except for $\bar{\Xi}$) differences are also predicted in the mid-rapidity interval. Despite the lower multiplicities this could be an interesting topic for future experiments.

Negative kaons are found to be more sensitive to the presence of a phase transition in the EOS than the positives ones, as well as the corresponding K^-/π^- ratio. The ratio K^+/π^+ has been compared with experimental data and both scenarios (specially the lattice one) are in good agreement with the measured ratios, a fact which again supports the assumption of an almost complete chemical equilibration. Differences between the positive and the negative ratios were found in both scenarios.

The rate Ξ^-/Λ was compared with experimental data (for $Si + Pb$) and is compatible with them. The results for both scenarios are not very different and therefore one concludes that this ratio involving a multi-strange hyperon does not appear to be a better signature then the $S = 1$ particle yields.

A particularly important aspect of this investigation is that the high negative pion multiplicity in this experiment can be obtained in a natural way just taking into account baryon and strangeness conservation, strangeness equilibration and resonance decays. It has its origin mainly in the Λ, Σ and Ξ channels, as I showed in detail in the previous section. The low m_t enhancement in π^- spectra can also be explained in this way.

Another step in the investigation of the equation of state which governs the heavy ions physics would be to realize the same simulation using an EOS based on lattice-QCD calculations extended into the baryonic sector.

References

[1] R. Hagedorn; Nuov. Cim. Suppl. 3(1965)147. J. Rafelski and R. Hagedorn; in Statistical Mechanics of Quarks and Hadrons, Bielefeld Symposium (1980), ed. H. Satz (North-Holland, Amsterdam, 1981), pg.253.

[2] N. Arbex, U. Ornik and R.M. Weiner; 'The Phase Transition in the SPS Energy Range' (in preparation).

[3] J. Bolz, U. Ornik, R.M. Weiner; Phys.Rev.C 46(1992)2047.

[4] BNL-AGS E802/866 Collaboration, Nucl.Phys. A590 (1995) 519c.

[5] L. Ahle et al., E866 Collaboration, Nucl.Phys. A590 (1995) 249c.

[6] R. Stock, GSI-Yellow Report, Darmstad 1981.

[7] T.A. DeGrand, Phys. Rev. D30(1984)2001.

[8] P. Koch, B. Müller and J. Rafelski, Phys.Rep.142 (1986)167.

[9] K.S. Lee, M. Rhoades-Brown and U. Heinz, Phys.Rev. C37(1988)1452.

[10] C. Greiner, P. Koch and H. Stöcker; Phys. Rev. Lett 58(1987)1825.

[11] S.E. Eiseman et al., Phys. Lett. B325(1994)322.

[12] T. Abbott et al.; Nucl. Phys. A498(1989)67c

[13] J. Cleymans, H. Satz, E. Suhonen and D.W. Von Oertzen; Phys. Lett B242(1990)111.

Chapter 5

π^-/π^+ Ratio in Heavy Ion Collisions:
Coulomb effect or chemical equilibration ?

Recently the NA44 Collaboration has presented results of measurements of π^-/π^+ ratios in heavy ion reactions at the CERN/SPS accelerator at incident beam energies of 158 and 200 GeV/A [1].

The observed excess of negative over positive pions in the low m_t region was interpreted in this report as due to Coulomb final state interactions, although no quantitative estimate of this effect has been given. Important arguments in this interpretation were the following:
(i) RQMD predictions, including the decays of resonances, could not account for this excess.
(ii) in $Pb + Pb$ reactions the effect is more pronounced than in $S + S$ reactions.

In this chapter I present a calculation of the pion ratios and of related particle yields for heavy ion collisions at CERN/SPS and BNL/AGS energies. In previous publications on 200 $AGeV$ $S + S$, 158 $AGeV$ $Pb + Pb$ and 11 $AGeV$ $Au + Au$ many different physical observables concerning these reactions was presented such as single inclusive spectra and pion correlations ([2]-[7] and Chapter 4). The present calculation is based on these previous simulations.

For the initial conditions of the fireball at SPS energies one had to take into account a certain degree of transparency of the colliding nuclei, whereas for the reaction at AGS energies one considered 3-d full-stopping from the moment of impact.

All the results presented here have been obtained by using the lattice-EOS and HYLANDER-PLUS version. The freeze-out temperature is chosen as $T_f = 139\ MeV$.

In the calculations for SPS energies I took into account the detector acceptance as defined in [1] and [8] [1].

[1] I find, e.g., that only about 17% of negative pions from Λ decay and about 15% of negative pions from Σ decay survive the detection conditions for the $Pb+Pb$ reaction. For the $S + S$ reaction the numbers are respectively 23% and 22%. However, the presented results for the pion ratio are not strongly affected by the limited detector acceptance.

In Section 1 the results are shown and Section 2 contains the discussion about the results [2].

1 Results

In Fig. 1 the results for $Pb+Pb$ and $S+S$ collisions at SPS energies are shown. They are compared to the data published in reference [1]. For $Pb+Pb$ collisions the simulation is compatible with the data (Fig.1(a)), while for $S+S$ collisions (Fig.1(b)) this is not the case: here the model predicts an enhancement as well, which is apparently not present in the data.

In Fig. 2 the π^-/π^+ ratio for $Au+Au$ collisions at AGS energies are presented. The results of the simulation are compared with preliminary data from reference [9]. Here the ratio reaches even bigger values than those found for $Pb+Pb(SPS)$ data. Below we will discuss possible reasons for this.

FIGURE 1

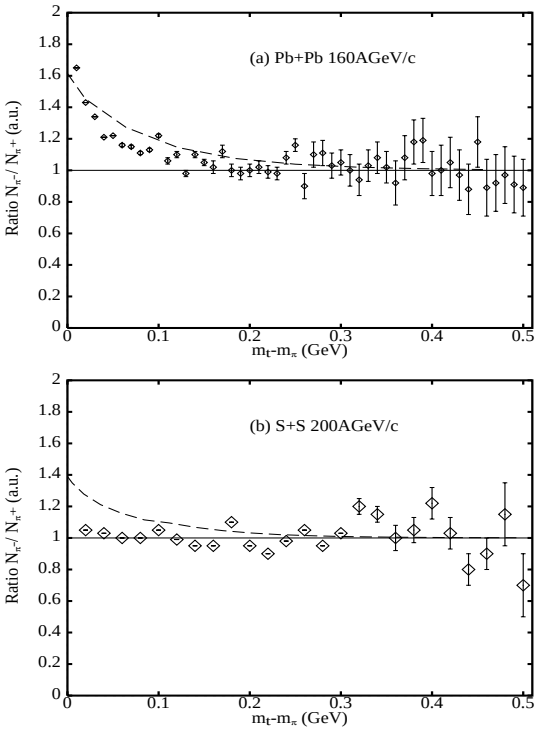

Fig. 1: π^-/π^+ ratio obtained from a (3+1) dimensional hydrodynamical simulation (HYLANDER -PLUS) in comparison to the data from ref.[1], (a) for $Pb+Pb$ collision and (b) for $S+S$ collision. Both cases refer to CERN/SPS energies.

[2] The results of this chapter have been published in Phys. Lett. B391 (1997) 465.

In the model, the low m_t enhancement in the π^- production is a consequence of nuclear stopping, thermalization, hadronization and chemical equilibration of the fireball produced in a relativistic heavy-ions collision. At the beginning, a large number of baryon stopped in the central region will thermalize. This induces a strange chemical potential which favours the production of hyperons (which are not present in the initial state). The number of hyperons reaches a maximum value if the equilibration is complete. After hadronization (freeze-out) the hyperons decay dominantly into $\pi^- + (p, n)$ channels. They are concentrated in the soft m_t region because of the low amount of available kinetic energy in the hyperon decay.

FIGURE 2

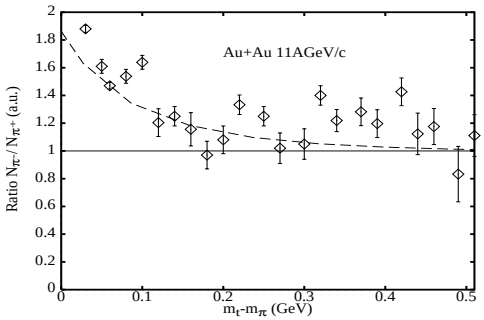

Fig. 2: π^-/π^+ ratio obtained from a (3+1) dimensional hydrodynamical simulation (HYLANDER -PLUS) in comparison to the data from ref. [9] for $Au + Au$ collision at BNL/AGS energies.

2 Discussion

I already analyzed the enhancement in the π^- production for $Au{+}Au$ in Chapter 4. I showed that taking into account baryon and strangeness conservation as well as strangeness equilibration, including the decay of resonances in the final stage, the difference $N_{\pi^-} - N_{\pi^+}$ in the model is determined by the amount of produced hyperons, i.e.,

$$N_{\pi^-} - N_{\pi^+} = N_{\text{ hyperons decaying into } \pi^-} - N_{\text{ hyperons decaying into } \pi^+} \quad (1)$$

We have [7] [3]:

$$N_{\pi^-} - N_{\pi^+} \simeq$$
$$0.64 N_\Lambda + N_{\Sigma^-(1190)} + 0.64 N_{\Sigma^0} - 0.48 N_{\Sigma^+} + 1.64 N_{\Xi^-} + 0.64 N_{\Xi^0} \quad (2)$$

[3] In this simulation I am considering resonances with masses up to 1.5 GeV. About 80% of the enhancement of the π^-/π^+ ratio is due to lambdas.

On the other hand, if the Coulomb effect would be the main mechanism in the observed excess and the resonance contribution would be of secondary importance, then the total number of π^- should be almost equal to the total number of π^+ and consequently there should appear at large m_t a compensating π^+/π^- excess. This means that the number of pions (or the pion ratio) at large m_t can help to distinguish between these two interpretations. Interestingly enough, up to $m_t - m_\pi = 0.8$ GeV the available $Au + Au$ data do not show an excess of π^+ over π^-. They also show that the total number of π^- is significantly larger than that of π^+ ($N_{\pi^-} - N_{\pi^+} \approx 40$ [9]) (For $Pb + Pb$ no such data are yet available).

I also find that the enhancement of the pion ratio depends on the final baryon density (and therefore on the final baryon chemical potential) of the fireball at freeze-out. The computed baryon density values at freeze out are: 0.072 n_0, 0.094 n_0 and 0.192 n_0 for $S+S(SPS)$, $Pb+Pb(SPS)$ and $Au + Au(AGS)$ respectively [4]. The reduction of the enhancement from AGS to SPS energies can therefore be interpreted as due to an increase of the transparency effect.

One should stress that the K^-/K^+ and $\bar{p}/p$ ratios as predicted by the model do not depend on m_t, in agreement with the results cited in [1]. Furthermore the same approach predicted and/or reproduced correctly the rapidity and transverse momentum spectra of protons and negative hadrons as well as the Bose-Einstein correlations in both $S+S$ and $Pb + Pb$ reactions at SPS energies. In $Au + Au$ at AGS energies it reproduces all single inclusive data (protons, negative and positive pions and kaons).

A possible interpretation of the results for $Pb + Pb$ reactions is that the Coulomb effect is in fact much smaller than expected in [1] and chemical equilibration has to be taken into account as an alternative explanation.

Finally I would like to comment on the fact that the model overestimates the 200 $AGeV$ $S + S$ pion ratio compared to the available data.

In [2] the lambda production was calculated for $S + S(SPS)$ considering the conditions described by NA35 Collaboration in [10]. The multiplicity calculated in this approach was 8.77 and the experimental value was 8.2 ± 0.9 [5].

Considering that the detection conditions permit the measurement

[4] n_0 is the normal baryon density $= 0.14/fm^3$.

[5] The NA35 Collaboration presented in a later paper [11] a new value for the Λ total multiplicity: 9.4 ± 1.0. In this experiment the Σ^0 were detected together with the Λ, so as in the calculation presented in [2].

of π^- from Λ decay, the overestimation in the pion ratio is surprising in so far as there appears to be agreement between the calculated Λ rate and the measured one (which suggests that a similar agreement might hold for the other, not yet measured, hyperon rates) and this would necessarily imply an excess of produced π^- compared with π^+ (see eq.(2)). However this model is based on the hypothesis of chemical equilibration at freeze-out, and the overestimate of the pion ratio for $S+S$ might indicate that a complete chemical equilibration in this system is not reached until freeze-out, whereas it is in $Pb+Pb$ and $Au+Au$. One expects that the bigger the system or the longer the life-time ($\tau_{(Pb+Pb)} \approx 14\ fm/c$, $\tau_{(S+S)} \approx 7\ fm/c$, $\tau_{(Au+Au)} \approx 10\ fm/c$) [2] [6][7] the higher the degree of chemical equilibration at freeze-out. This would indicate that the π^-/π^+ ratio is more sensitive to the establishment of chemical equilibrium than other physical observables. However I believe that such a conclusion, although extremely interesting and of possible practical value, might be premature, because it strongly depends on the accuracy of preliminary $S+S$ data.

In order to obtain a clarification of the issues raised above the following experimental steps appear necessary:
(a) Determination of all accessible hyperon rates in $S+S(SPS)$, $Pb+Pb(SPS)$ and $Au+Au(AGS)$ reactions.
(b)Measurements of the π^-/π^+ ratio at large m_t in all three reactions.
(c) Remeasurements of the π^-/π^+ ratio in $S+S(SPS)$ at low m_t.

References

[1] H. Bøggild et al.; Phys. Lett. B372 (1996) 343.

[2] J. Bolz, U. Ornik and R.M. Weiner; Phys.Rev. C46 (1992) 2047.

[3] J. Bolz, U. Ornik, M. Plümer, B.R. Schlei and R.M. Weiner; Phys.Lett B300 (1993) 404.

[4] J. Bolz, U. Ornik, M. Plümer, B.R. Schlei and R.M. Weiner; Phys.Rev. D47 (1993) 3860.

[5] N. Arbex, U. Ornik, M. Plümer, A. Timmermann and R.M. Weiner.; Phys. Lett. B345 (1995) 307.

[6] B.R. Schlei, U. Ornik, M. Plümer, D. Strottman and R.M. Weiner, Phys. Lett. B376 (1996) 212; U. Ornik, B. R. Schlei, M. Plümer, D. Strottman and R. M. Weiner, Phys. Rev. C54 (1996)1381.

[7] N. Arbex, U. Ornik, M. Plümer and R.M. Weiner; Phys. Rev. C55 (1997) 860.

[8] see, for example, H. Bøggild et al, Phys. Lett. B 302(1993) 510 and Nu Xu in 'Quark Matter 96'.

[9] L. Ahle et al.; Nucl.Phys. A590 (1995) 249c.

[10] J. Bartke et al.; NA35 Collaboration, Z. Phys. C48 (1990) 191.

[11] T. Alber et al; NA35 Collaboration, Z.Phys. C64 (1994) 195.

Chapter 6
Thermal Photon Production

In ultrarelativistic heavy-ion collisions one of the most challenging goals is to study a possible phase transition between nuclear matter and the quark-gluon-plasma (QGP). This expectation is supported by lattice gauge calculations and phenomenological models (Chapter 1). Photons are a very promising probe in the experimental search for the QGP which is expected to exist for a brief period of a few fm/c before the majority of the final state hadrons is emitted (see also Appendix 2). Particles which interact only electromagnetically may be regarded as free particles, carrying information on the early stage of the collision.

I already mentioned that for heavy ion collisions at the Brookhaven Alternating Gradient Synchrotron (AGS) and at the CERN Super Proton Synchrotron (SPS) the assumption of thermalization may be fulfilled because of the high degree of stopping. Thus, high compression of nuclear matter has to be considered and energy densities near the critical value for the deconfinement phase transition may be reached.

In the present chapter, a study of thermal photon production and predictions for measurements at AGS and SPS energies is presented. The results are focused on the reactions $Au + Au$ at $E_{lab} = 11.5$ AGeV and $Pb + Pb$ at 160 AGeV. The model is also applied to $S + Au$ collisions at 200 AGeV and the results are compared to preliminary data on photon production obtained by the WA80 Collaboration [1].

At the SPS direct photon production will be performed by the WA98 Collaboration [2]. Furthermore, it is intended [3] to test the PHENIX-detector [4], which is designed to detect photons with high accuracy and resolution at the AGS. This means that the predictions for $Pb + Pb$ at 160 AGeV and for $Au + Au$ at 11.5 AGeV can be checked in the near future.

In the first Section I present the results and in the second discussions of the results [1].

1 Calculations and Results

The photon production rates in thermalized matter have been calculated both for a QGP and for a hadron gas. In a QGP of temperature

[1] These results have been published in Phys. Lett. B345(1995) 307.

T, the rates for a baryochemical potential $\mu = 0$ can be expressed as [5]:

$$E_\gamma \frac{dN}{d^3k d^4x} = \frac{5}{18\pi^2} \alpha \alpha_s T^2 e^{-E_\gamma/T} \ln \frac{0.2317 E_\gamma}{\alpha_s T}. \tag{1}$$

where E_γ and $\vec{k}$ are the energy and three-momentum of the photon, and where $\alpha = 1/137$ and α_s are the electromagnetic and the temperature dependent strong coupling constant, respectively. From lattice results $\alpha_s(T)$ can be parametrized as [6]:

$$\alpha_s(T) = \frac{6\pi}{(33 - 2n_f)\ln(8T/T_c)}. \tag{2}$$

where T_c is the critical temperature and n_f is the number of flavors (below, one takes $n_f = 2$).

For a hadronic resonance gas at temperature T and baryochemical potential $\mu = 0$, the thermal photon rates were calculated in [7]. The authors of [7] parametrized their results in the form

$$E_\gamma \frac{dN}{d^3k d^4x} = 2.4\, T^{2.15} \exp\left[\frac{-1}{(1.35 T E_\gamma)^{0.77}} - \frac{E_\gamma}{T}\right] \qquad [GeV^{-2} fm^{-4}], \tag{3}$$

where E_γ and T are measured in units of GeV. Eq. (3) contains the contributions from A_1-resonances which were shown to be important in [7] and which had not been taken into account in earlier calculations of the rates [8].

In the mixed phase the rates read

$$E_\gamma \frac{dN}{d^3k d^4x}\bigg|_{mix} = w(\varepsilon)\, E_\gamma \frac{dN}{d^3k d^4x}\bigg|_{QGP} + (1 - w(\varepsilon))\, E_\gamma \frac{dN}{d^3k d^4x}\bigg|_{had}. \tag{4}$$

where $w(\varepsilon)$ is the fraction of QGP at the energy density ε.

In order to obtain the single-inclusive spectra it is necessary to integrate the photon rates over the space-time region defined by the space-time evolution of the hot and dense matter,

$$E_\gamma \frac{dN}{d^3k} = \int d^4x E_\gamma \frac{dN}{d^3k d^4x} (T(x), u^\mu(x)) \qquad , \tag{5}$$

where the temperature field $T(x)$ and the four velocity field $u^\mu(x)$ are obtained from a hydrodynamic description of the expanding matter. On the rhs of eqs. (1) and (3) the energy E_γ has to be replaced by $k_\mu u^\mu(x)$.

The space-time development of dense and hot matter in local thermal equilibrium is described by the equations of relativistic hydrodynamics solved by HYLANDER-PLUS.

The hydrodynamical simulation presented here describes also the initial compression stage where the propagation of shock waves which heat up the system is calculated fully 3-dimensionally, using the new initial condition option of the new version explained in Chapter 3.

I use the lattice-EOS. Apart from the EOS, the hydrodynamic simulations do not contain any free parameters.

Fig. 1 shows the first 8 fm/c of the space-time evolution of central $Au+Au$ collisions at $E_{lab} = 11.5$ AGeV (left column) and of central $Pb+Pb$ collisions at 160 AGeV, in time steps $\Delta t = 2$ fm/c. Contour plots for the energy-density calculated with HYLANDER-PLUS are displayed. Four characteristic regimes are considered. The energy density $\varepsilon = 0.14$ GeV/fm^3 corresponds to the interface between hot and cold nuclear matter, $\varepsilon = 0.25$ GeV/fm^3 to the freeze out regime, the region $2.5 \leq \varepsilon \leq 5.5$ GeV/fm^3 to the mixed phase and $\varepsilon \geq 5.5$ GeV/fm^3 to the pure QGP phase, respectively. As can be seen in the figure, for both reactions a lump of pure QGP and a mixed phase with a lifetime of about 7 fm/c are produced. The total lifetimes of the thermalized matter are ~ 10 fm/c for $Au + Au$ at 11.5 AGeV and ~ 16 fm/c for $Pb + Pb$ at 160 AGeV.

Figs. 2a and 2b show the thermal photon spectra for these two reactions. The rates are surprisingly large even at AGS energies. To understand the origin of these results, I have plotted separately the contributions from the pure QGP phase, the mixed phase and the purely hadronic phase. For $Au + Au$ at 11.6 AGeV the contribution of the purely hadronic phase dominates the photon production, whereas for $Pb + Pb$ at 160 AGeV it is comparable to the contribution of the pure QGP phase.

The reason that the pure hadronic phase plays such an important role in photon production is twofold. Firstly, as can be seen from eqs. (1) and (3), at temperatures $T \sim 0.2$ GeV the hadron gas outshines the QGP by a factor of about two. Secondly, the hadronic space-time volume exceeds the volumes occupied by the mixed phase and by the QGP. The fact that at SPS energies the QGP contribution can compete with that of pure hadronic phase is a consequence of the high initial temperatures ($T_i \sim 300$ MeV) at these energies.

Preliminary data on photon production for $S + Au$ collisions at SPS energies were recently presented by the WA80 Collaboration [1]. The fact that the measured direct photon rates are surprisingly high has led to speculations concerning the existence of an extremely long-lived mixed phase with lifetimes of about $30 - 40$ fm/c[9].

Fig.1

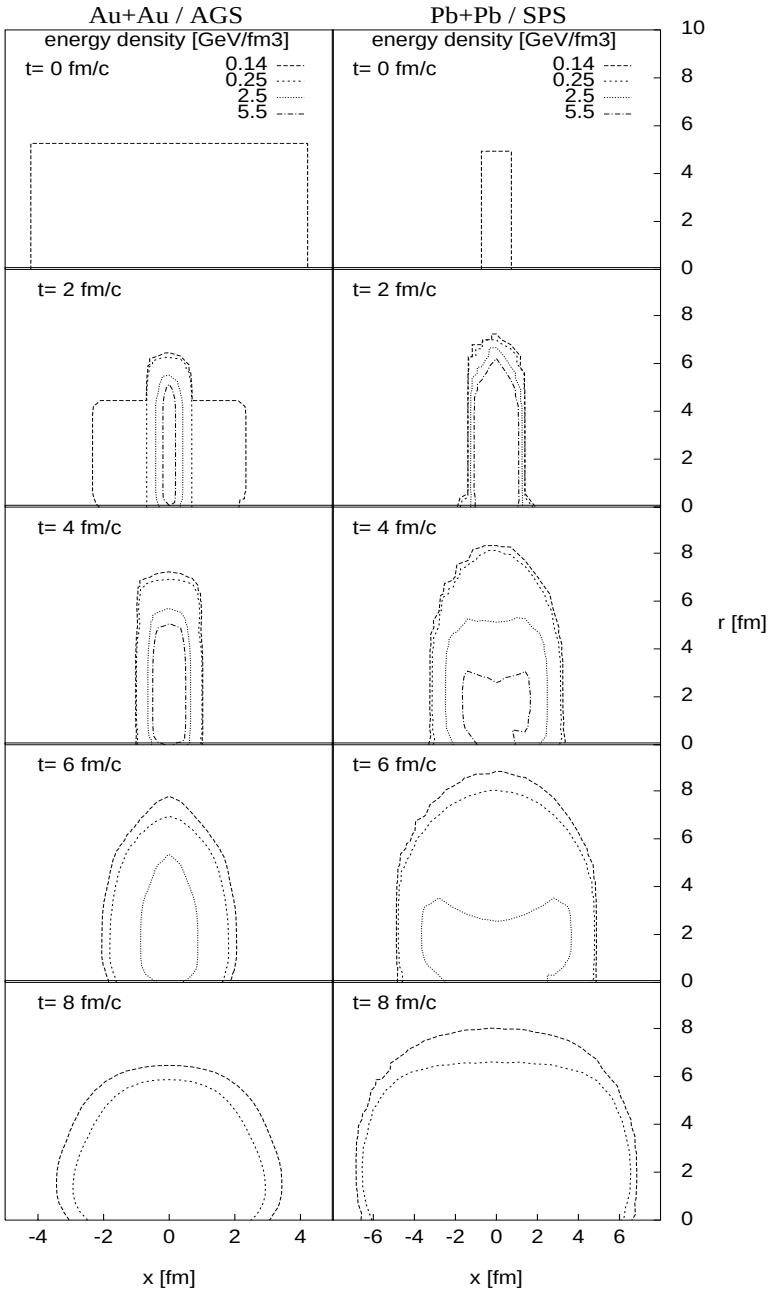

Fig. 1: Energy density contour plots in the (x, r) plane, for $Au + Au$ collisions at $E_{lab} = 11.5$ AGeV (left column) and $Pb + Pb$ collisions at $E_{lab} = 160$ AGeV (right column). x is the coordinate in longitudinal direction, r the radial coordinate in the transverse plane. The plots were obtained in the equal velocity frame by applying the hydrodynamic collision simulation.

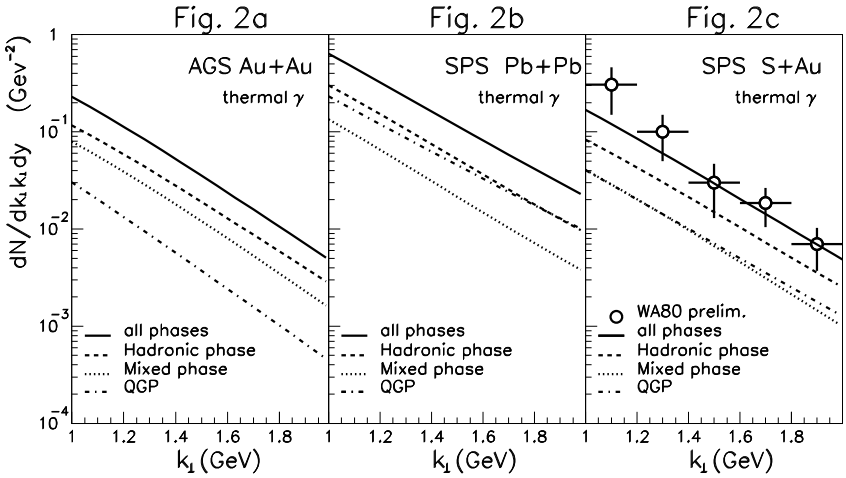

Fig. 2: Single-inclusive photon spectra as a function of the transverse momentum $k_\perp$ for mid-rapidity photons, (a) for $Au + Au$ collisions at $E_{lab} = 11.5$ AGeV, (b) for $Pb + Pb$ at 160 AGeV and (c) for $S + Au$ at 200 AGeV. The contributions from the pure QGP phase, the mixed phase and the pure hadronic phase are shown separately. The data points are from ref. [1].

The hydrodynamic simulation is applied to this reaction[2] and the resultant thermal photon rates plotted in Fig. 2c. A remarkably good agreement with the WA80 data [1] is found, without having to adjust any parameters or having to assume an extremely long-lived mixed phase as in Ref. [9]. In particular, it turns out that the hadronic rather than the mixed phase dominates photon emission.

The space-time evolution for $S + Au$ collisions is illustrated in Fig.3. Due to asymmetry of the collision, the central rapidity region is shifted, which is of importance for the calculation of the photon spectra.

2 Discussion

An analysis about the importance of each phase of the development of the fireball to calculate photon production in heavy ions reactions at different energy ranges was made using the model and some discussion about the results were presented in the last section. There is one aspect more to discuss: the effects of baryon stopping on thermal photon production.

[2] For the system $S + Au$ one expects a smaller degree of stopping than for $Pb + Pb$ or $Au + Au$. On the other hand, fits to rapidity and transverse momentum spectra of hadrons produced in $S + S$ at 200 AGeV already indicate a considerable amount of stopping [10] which should be even more pronounced for $S + Au$. This suggests that the hydrodynamic simulation for full-stopping case is also applicable for the latter reaction. Note, however, that recently the WA80 data have also been described [11, 12] under the assumptions of Bjorken initial conditions.

Fig.3

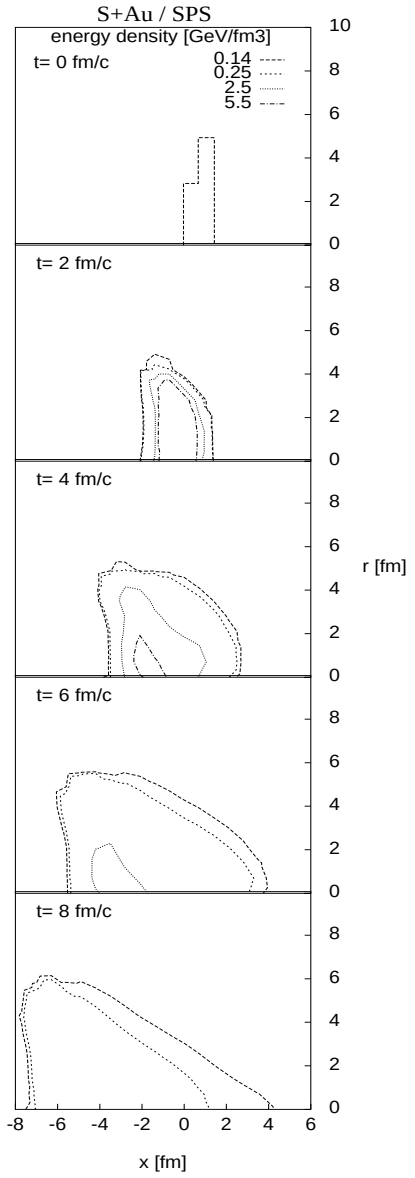

Fig.3: Energy density contour plots as in Fig.1 for $S+Au$ collisions at E_{lab} =200 $AGeV$.

At AGS and SPS energies, one expects nonvanishing values of the baryochemical potential due to the high baryon number densities in the central rapidity region. In Ref. [13], photon emission rates from a QGP of temperature T and baryochemical potential μ were calculated by means of the Braaten-Pisarski technique. The authors give the

expression

$$E_\gamma \frac{dN}{d^3k d^4x} = \frac{5}{18\pi^2}\alpha\alpha_s T^2(1+\frac{\mu^2}{\pi^2 T^2})e^{-E_\gamma/T}\ln\frac{0.2317E_\gamma}{\alpha_s T}. \qquad (6)$$

At fixed baryon number density and energy density, I have used a bag model EOS with $T_c(\mu = 0) = 0.2$ GeV to estimate the decrease in temperature and the resultant decrease in the photon rates [14, 13] near the critical curve of the deconfinement phase transition. Using eqs. (6) and (3) one obtains reduction factors of about 2 both for the QGP and for the hadronic component[3].

From the above considerations one concludes that the main result of this investigation – namely, that there are experimentally observable rates of thermal photons to be expected both at the AGS and at the SPS – remains unaffected if one takes into account a finite baryochemical potential.

[3] A reduction by a factor of ~ 2 for $S + Au$ at 200 AGeV would imply that the calculation underestimates the WA80 data. There are two possible effects which would lead to an increase of the photon rates and thus may explain the missing factor. An additional contribution is also expected from the hadronic process $A_1 \to \pi\gamma$, $b_1 \to \pi\pi^0\gamma$ and $K_1 \to K\gamma$ [15]. Furthermore at nonzero baryochemical potential the presence of baryons may open additional channels for thermal photon production. Thirdly, one expects a decrease of the rho meson mass as the temperature approaches the critical temperature of the chiral phase transition[16].

References

[1] R. Santo et al., WA80-Collaboration, Nucl. Phys. A566 (1994) 61c.

[2] Experiments at CERN in 1993, CERN, Nov. 1993, ISSN 0259-093X.

[3] M. Tannenbaum, private communication.

[4] S. Nagamiya, Nucl. Phys. A566 (1994) 287c.

[5] J. Kapusta, P.Lichard, D. Seibert; Phys.Rev.D 44(1991)2774.

[6] F. Karsch; Z.Phys. C38 (1988) 147.

[7] L. Xiong, E.Shuryak and G.E. Brown; Phys.Rev.D 46(1992)3798.

[8] H. Nadeau, J. Kapusta and P. Lichard, Phys. Rev. C45 (1992) 3034.

[9] L.Xiong, E. Shuryak, Phys. Lett. B333 (1994) 316.

[10] J.Bolz, U.Ornik, R.W.Weiner; Phys.Rev.C 46 (1992) 2047.

[11] J.J. Neumann, David Seibert, George Fai, Preprint KSUCNR-016-94 (1994).

[12] D.K. Srivastava and B. Sinha, Phys. Rev. Lett. 73 (1994) 2421.

[13] C.T. Traxler, H. Vija, M.H. Thoma; Preprint UGI-94-14.

[14] A. Dumitru et al., Mod. Phys. Lett. A8 (1993) 1296.

[15] K. Haglin, Preprint MSCUCL-926 (1994).

[16] G.E. Brown and Mannque Rho, Phys. Rev. Lett. 66 (1991) 2720.

Chapter 7
Conclusions and Perspectives

Based on the results of the simulations and discussions I would like to present some general conclusive remarks.

This dissertation contributes to prove that the relativistic hydrodynamics is an important approach to study heavy ion collisions at high energy. The exact (3+1) dimensional numerical solution of the relativistic hydrodynamical equations is an essential instrument to describe strongly interacting many particle systems and hadronic multiparticle production.

This model was able to describe data from symmetrical and asymmetrical collisions regarding protons, $\pi^{\pm}$, $K^{\pm}$, heavy baryons, anti-heavy baryons and photons (leptons) production, at SPS and at AGS energy ranges.

Thanks to the new version, the number of free parameters in the simulation was reduced to the ones in the EOS, creating a method to analyze the influence of the existence of a QGP phase on particle production/spectra, what also permits to thoroughly test the hydrodynamical model.

Concerning the questions about the physics involved in nucleus-nucleus collisions, a summary will be presented below:

a) Thermalization and Stopping:

The results obtained here and in other studies suggest that the experimental data is in agreement with the assumption of thermalization of the system during the compression stage of the reaction.

The amount of stopping tells us how much energy in the reaction is available for thermalization. The simulations and the comparisons of obtained results with experimental data showed that the amount of energy available for thermalization is between 70% (S+S at SPS) and 100% (Au+Au at AGS and asymmetrical collisions) of the initial available energy.

b)Chemical equilibration and phase transition:

The problem of chemical equilibration is not yet solved. It is expected that chemical equilibrium can be much easier achieved if the fireball spent some time of its evolution in the QGP phase, because in this

phase all quarks are massless and especially strange matter is assumed to be produced faster than in the hadronic phase [1].

In this dissertation the assumption was made that the system achieved local chemical equilibration, for any EOS. From the results showed in Chapter 4 and 5 a possible conclusion is that the ratios Ξ^-/Λ, π^+/K^+ and π^-/π^+ are good signals to check the assumption of achievement of chemical equilibration in the reactions.

Some special attention should be given to data on π^-/π^+ ratio from S+S collisions. In Chapter 5 was shown that the published experimental data is not in agreement with the calculated ratio from the simulation and one possible explanation for this would be that chemical equilibration had not been achieved in this reaction. This explanation is, however, in contradiction with the general description obtained for the first data generation and the measured Λ production , from where the excess of π^- over π^+ production could come. One aspect to take into account is that the first data generation (which showed spectra for negative hadrons and protons) obtained the proton spectra by subtracting the number of negatively charged particles from the positively charged ones. This was done under the assumption that an equal number of π^- and π^+ was produced. According to what I demonstrated in Chapter 4 and 5 this hypothesis is probably wrong, the difference between total number of negative and positive produced pions depends on the number of produced heavy baryons. The data analysis made for $S + S$ under such hypothesis should be rechecked.

The excess of π^- relative to π^+ total production, confirmed by the experimental data for $Pb + Pb$ and $Au + Au$ reactions, can not be explained considering Coulomb effect to interpret the data. If the pion contribution from resonance decays would be of secondary importance, the total number of positive and negative produced pions would be the same. Consequently, a compensating effect should appear in the π^-/π^+ ratio at large m_t.

In order to complete this discussion, one should mention that there are some controversies about the composition of negative pions data from $S + S$ and $Pb + Pb$ experiments with regards to the measurement of negative pions from Λ decay. The results presented here consider the characteristics of the detection system of these experiments and is also based on discussions with experimentalists. From that I assumed that

[1] It was argued in [1] that a partial restoration of chiral symmetry with the increase of temperature in the hadronic phase might lead to a decrease of the strange particle masses and therefore could cause strangeness equilibration even in the hadronic phase. See however [2] where an opposite behaviour of kaon masses with temperature is expected.

the pions from this decay were included in the data (with an efficiency determined by experimental conditions) and this aspect is an important part of the data interpretation presented about this subject.

To clarify this discussion I suggested: a) determination of all accessible hyperon rates from $S + S$, $Pb + Pb$ and $Au + Au$ reactions; b) measurements of π^-/π^+ ratio at large m_t and c) remeasurement of π^-/π^+ in $S + S$ collisions.

Now we turn our attention to the sensitivity of data to the presence of a QGP phase. The EOS based on lattice results containing a first order phase transition from QGP to hadronic phase have provides an overall better description of the data for $Au + Au$, $S + S$, $Pb + Pb$ and also photon production for $S + Au$ was evaluated using this EOS.

The study presented in Chapter 4 for Au+Au (AGS) showed that an EOS without phase transition, containing resonances with masses up to 2 GeV can also describe proton and pions spectra [2]. The presence of a QGP phase influences the calculated total number of almost all produced particles and especially K^- spectra. Since kaon production is linked to hyperon production, the sensitivity of hyperon production/spectra was checked. An analysis of the rapidity spectra for hyperons and anti-hyperons showed that the influence of the QGP phase can be observed in the rapidity range $y > 1$. This is also true for Δ and $\bar{\Delta}$ production. Total multiplicity of Ξ, Ω, $\bar{p}$ and $\bar{\Delta}$ are also very sensitive.

These results could indicate that the answer to the question about QGP signatures is to be found in kaons, heavy baryons and heavy anti-baryons spectra. Careful studies on these data are very important and should be a goal for the next experiments, despite the lower multiplicities.

These conclusions also suggest new research directions.

The data descriptions presented in this dissertation and the previous studies using the first version of HYLANDER-PLUS encourage us to continue investigating heavy ion collisions at high energies using this hydrodynamical model.

With the possibility to investigate the influence of the phase transition on particle production without free parameters (apart from the ones in the EOS) and to calculate production of many observables, the aim of the investigation can be clearly amplified.

This method of investigation can be applied to analyze all heavy ion

[2] As already mentioned, there are problems to understanding chemical equilibration in this scenario. Further studies on this aspect are necessary involving simulations of other experiments, in order to check the behaviour of production of these particles in the presence of a phase transition.

experiments at AGS energy range and all asymmetrical cases involving heavy ions at SPS energies In these scenarios the full-stopping condition seems to be realistic.

Studies on experiments at SPS energies (which present lower levels of stopping) using this method should be also done, in order to investigate the hypothesis of full-stopping and its influence on the development of the fireball and particle production in such reactions.

The next generation of experiments at RHIC (Relativistic Heavy Ion Collider), which will have even higher energy available for the collision, represent a challenge in the investigation of heavy ions high energy physics. We are able to simulate this experiment, assuming different amounts of stopping and different EOS, and calculate the production of many observables. This would be important for the construction of the new detection systems.

References

[1] G. E. Brown et al., Phys. Rev. C43 (1991) 1881.

[2] J. P. Blaizot and R. Mendez Galain, Phys. Lett. B271 (1991) 32.

Chapter 8

Higher Order Bose-Einstein Correlations:
a test for the Gaussian density matrix assumption

Bose-Einstein Correlations (BEC) are the basis of an experimental method for the determination of sizes and lifetimes of sources in particle and nuclear physics. This knowledge is essential for an understanding of the dynamics of strong interactions.

A particularly important aspect of BEC is represented by higher order correlations because of the prediction, which follows from the gaussian density matrix assumption, that all higher order moments of the current distribution can be described in terms of the first two. The gaussian form (in the coherent state representation) of the density matrix [1] is a fundamental assumption of BEC and follows from the central limit theorem for a large number of independent sources, which are expected to act in a high energy reaction. Furthermore, higher order correlations provide important constraints on the space-time form of the sources, their dynamics (expansion) and chaoticity.

Experimentally correlations of three and more particles have been studied in the last years in [1]-[11] and more recently attempts have been made to analyze these correlations in terms of simplified models [12]-[15] without clear space-time implications for the emitting source (sources). Usually gaussian or exponential forms for the correlation functions in momentum space are postulated. In contrast to this, the approach used in this work starts with the space-time characteristics of an expanding source and the space-time form of the correlators within the classical current formalism. The dependence of C_n on the four-momentum difference (Q) follows after explicit integration over space-time variables [16].

The aim of this investigation is to use the higher order correlations NA22 data to test the validity of the gaussian density matrix assumption, within the space-time approach to BEC.

[1] The mathematical form of the density matrix must not be confused with the form of the correlator or of the space-time distribution of the source, cf.below.

1 The General Formalism

1.1 First principles

In quantum mechanics, a multiparticle production process is described in terms of a density matrix $\hat{W}$ which characterizes the final state of the system. From the density matrix, all n-particle distributions can be determined, and conversely, a measurement of these distributions yields information about the density matrix of the multiparticle system. The n-particle inclusive distribution is defined through the creation and annihilation operator $a_i^\dagger(\mathbf{k})$ and $a_i(\mathbf{k})$ of a particle of momentum k (i labels internal degrees of freedom):

$$\rho_n^{i_1\ldots i_n}(\mathbf{k_1},\ldots,\mathbf{k_n}) \equiv \frac{1}{\sigma}\frac{d^n\sigma^{i_1\ldots i_n}}{d\omega_1\ldots d\omega_n} = (2\pi)^{3n}\prod_{j=1}^{n} 2E_j Tr(\hat{W}a_{i_j}^\dagger(\mathbf{k_1})\ldots a_{i_n}^\dagger(\mathbf{k_n})a_{i_n}(\mathbf{k_n})\ldots a_{i_1}(\mathbf{k_1})) \quad (1)$$

where,

$$d\omega_i = \frac{d^3k_i}{(2\pi)^3 2E_i} \quad (2)$$

is the invariant volume in momentum space.

The general n-particle correlation function is defined as

$$C_n^{i_1\ldots i_n}(\mathbf{k_1},\ldots,\mathbf{k_n}) = \frac{\rho_n^{i_1\ldots i_n}(\mathbf{k_1},\ldots,\mathbf{k_n})}{\rho_1^{i_1}(\mathbf{k_1})\ldots\rho_1^{i_n}(\mathbf{k_n})} = 1 + \frac{\bar{C}_n^{i_1\ldots i_n}(\mathbf{k_1},\ldots,\mathbf{k_n})}{\rho_1^{i_1}(\mathbf{k_1})\ldots\rho_1^{i_n}(\mathbf{k_n})}. \quad (3)$$

In order to determine the density matrix for a given reaction from first principles, one would have to specify the initial state of the projectile and target and then apply the S matrix to this state. In general this is not possible. One way to proceed is to parametrize $\hat{W}$ according to a reasonable phenomenological description of the system. For this, one uses the external source (current) formalism. In this approach particle sources are treated as external classical currents, and their fluctuations are described by a gaussian distribution. This last choice can be justified by the fact that, if one has a superposition of N independent sources, the gaussian form follows from the central limit theorem in the limit of large N.

In the following we will also consider correlation functions as functions of Q^2 : [2]

[2] As usual, $Q_n^2 = \sum_{i<j}^n q_{ij}^2$; $q_{ij}^2 = -(k_i - k_j)^2$; $n \geq 2$ and $i, j = 1, \ldots, n$.

$$C_n(Q^2) = 1 + \frac{I_n(Q^2)}{I'_n(Q^2)} \tag{4}$$

with $(i, j = 1, ..., n)$,

$$I_n(Q^2) = \int dw_i ... \int dw_n \, \bar{C}_n^{i_1 ... i_n}(k_1, ..., k_n) \, \delta[Q^2 + \sum_{i,j=1(i<j)}^{n} (k_i - k_j)^2] \tag{5}$$

$$I'_n(Q^2) = \int dw_i ... \int dw_n \, \rho_1^{i_1}(k_i) ... \rho_1^{i_n}(k_n) \, \delta[Q^2 + \sum_{i,j=1(i<j)}^{n} (k_i - k_j)^2] \tag{6}$$

1.2 Higher order correlation functions

Here we give a brief summary of the derivation of Bose-Einstein correlation functions in the current formalism [17].

The current can in general be written as the sum of a chaotic and a coherent component, $J(x) = J_{chaotic}(x) + J_{coherent}(x)$. The Gaussian current distribution is completely specified by its first two moments: $I(x) \equiv < J(x) > = J_{coherent}(x)$ and the two-current correlator $D(x, y) \equiv < J(x)J(y) > - < J(x) >< J(y) >$.

$I(x)$ and $D(x, y)$ can be parametrized as $I(x) \propto f_c(x)$ and $D(x, y) \propto f_{ch}(x)C(x - y)f_{ch}(y)$, where $f_c(x)$ and $f_{ch}(x)$ are the space-time distributions of the coherent and the chaotic components of the source. The primordial correlator $C(x - y)$ reflects intrinsic dynamical properties of the source. It contains some characteristic length (or time) scales L, so-called correlation lengths (for a system in thermal equilibrium the correlation length can be related to the inverse of the temperature).

In the general case of a partially coherent source, the single inclusive distributions of pions can be expressed also as a sum of a chaotic and coherent component $(i = +, -, 0)$:

$$\frac{1}{\sigma}\frac{d\sigma^i}{d\omega} = \left.\frac{1}{\sigma}\frac{d\sigma^i}{d\omega}\right|_{chaotic} + \left.\frac{1}{\sigma}\frac{d\sigma^i}{d\omega}\right|_{coherent} \tag{7}$$

where,

$$\left.\frac{1}{\sigma}\frac{d\sigma^i}{d\omega}\right|_{chaotic} = D(k), \tag{8}$$

$$\left.\frac{1}{\sigma}\frac{d\sigma^i}{d\omega}\right|_{coherent} = |I(k)|^2. \tag{9}$$

$I(k)$ and $D(k)$ are the on-shell Fourier transforms of $I(x)$ and $D(x,y)$, respectively.

In general, the chaoticity parameter will be momentum-dependent:

$$p(k) = \frac{D(k)}{D(k) + |I(k)|^2}. \tag{10}$$

To write down the correlations functions in a concise form one introduces the normalized current correlator:

$$d_{rs} = \frac{D(k_r, k_s)}{[D(k_r, k_r).D(k_s, k_s)]^{1/2}} \tag{11}$$

where the indices r, s label the particles. Since $d(k_r, k_s)$ is in general a complex number, one may prefer to express the correlation functions in terms of the magnitudes and the phases of d_{rs},

$$T_{rs} \equiv T(k_r, k_s) = |d(k_r, k_s)|, \tag{12}$$

$$\phi^{ch}_{rs} \equiv \phi^{ch}(k_r, k_s) = \arg d(k_r, k_s) \tag{13}$$

and the phase of the coherent component

$$\phi^{co}_r \equiv \phi^{co}(k_r) = \arg I(k_r). \tag{14}$$

With this notation we write the chaoticity parameter: $p_r \equiv p(k_r)$.

The normalized cumulant correlation functions H_n for identical charged particles are:

$$H_2^{++}(k_1, k_2) = 2\sqrt{p_1(1-p1)p_2(1-p_2)}T_{12}cos(\phi^{ch}_{12} - \phi^{co}_1 + \phi^{co}_2) + p_1 p_2 T_{12}^2 \tag{15}$$

$$\begin{aligned} H_3^{+++}(k_1, k_2, k_3) = \frac{1}{3}p_1 p_2 p_3 T_{12} T_{23} T_{31} cos(\phi^{ch}_{12} + \phi^{ch}_{23} + \phi^{ch}_{31}) \\ +\sqrt{p_1(1-p1)p_2^2 p_3(1-p_3)}T_{12}T_{23}cos(\phi^{ch}_{12} + \phi^{ch}_{23} + \phi^{co}_3 - \phi^{co}_1) \\ \text{+permutation of 1,2,3} \end{aligned} \tag{16}$$

$$\begin{aligned} H_4^{++++}(k_1, k_2, k_3, k_4) = \\ \frac{1}{4}p_1 p_2 p_3 p_4 T_{12} T_{23} T_{34} T_{41} cos(\phi^{ch}_{12} + \phi^{ch}_{23} + \phi^{ch}_{34} + \phi^{ch}_{41}) \\ +\sqrt{p_1(1-p1)p_2^2 p_3^2 p_4(1-p_4)}T_{12}T_{23}T_{34}cos(\phi^{ch}_{12} + \phi^{ch}_{23} + \phi^{ch}_{34} + \phi^{co}_4 - \phi^{co}_1) \\ \text{+permutation of 1,2,3,4} \end{aligned} \tag{17}$$

The correlation functions C_n (3) can be expressed in terms of H_n by using the relation between the corresponding generating functionals [17]:

$$C_2^{i_1,i_2}(k_1,k_2) = 1 + H_2^{i_1,i_2}(k_1,k_2) \tag{18}$$

$$C_3^{i_1,i_2,i_3}(k_1,k_2,k_3) = \\ 1 + H_2^{i_1,i_2}(k_1,k_2) + H_2^{i_2,i_3}(k_2,k_3) + H_2^{i_3,i_1}(k_3,k_1) + H_3^{i_1,i_2,i_3}(k_1,k_2,k_3) \tag{19}$$

$$\begin{aligned} C_4^{i_1,i_2,i_3,i_4} \quad (\quad & k_1,k_2,k_3,k_4) = \\ 1 \quad + \quad & H_2^{i_1,i_2}(k_1,k_2) + H_2^{i_1,i_3}(k_1,k_3) + H_2^{i_1,i_4}(k_1,k_4) + H_2^{i_2,i_3}(k_2,k_3) \\ + \quad & H_2^{i_2,i_4}(k_2,k_4) + H_2^{i_3,i_4}(k_3,k_4) \\ + \quad & H_2^{i_1,i_2}(k_1,k_2).H_2^{i_2,i_3}(k_2,k_3) + H_2^{i_1,i_3}(k_1,k_3).H_2^{i_2,i_4}(k_2,k_4) \\ + \quad & H_2^{i_1,i_4}(k_1,k_4).H_2^{i_2,i_3}(k_2,k_3) \\ + \quad & H_3^{i_1,i_2,i_3}(k_1,k_2,k_3) + H_3^{i_1,i_2,i_4}(k_1,k_2,k_4) + H_3^{i_1,i_3,i_4}(k_1,k_3,k_4) \\ + \quad & H_3^{i_2,i_3,i_4}(k_2,k_3,k_4) + H_4^{i_1,i_2,i_3,i_4}(k_1,k_2,k_3,k_4) \end{aligned} \tag{20}$$

As one can see, all correlation functions depend only on the functions $T_{r,s}$, $\phi_{r,s}^{ch}$ and ϕ_r^{co} which will be specified in the next section for an expanding source.

Formally the results of the optical momentum-space model of [15], in particular eqs. (20-22) of that reference follow from the above equations in the assumption of a constant chaoticity p. Moreover assuming real fields (currents) and symmetrical momentum-space or space-time configurations (T_{rs} independent of r,s) it follows from the above equations that all correlations C_n with $n \geq 3$ depend only on two quantities p and T_{12} which can be determined from the first two correlation functions. This by now well known result imposes stringent (possibily too stringent, cf. below) constraints on C_n.

1.3 The expanding source

For the space-time description of an expanding source is useful to define variables τ, η and $x_{||}$:

$$\tau = \sqrt{x_0^2 - x_{||}}, \qquad \eta = \frac{1}{2} ln \frac{x_0 + x_{||}}{x_0 - x_{||}} \tag{21}$$

where τ is the proper-time, $x_{||}$ the coordinate in the direction of the collision axis and η the space-time rapidity. Here we will consider invariance under boosts of the coordinate frame in the longitudinal direction, which

corresponds to the assumption that the single inclusive distribution in rapidity is flat.

The space-time distribution of the chaotic and coherent source, as well as the primordial correlator [3], are expressed in terms of 10 parameters: $\tau_{0,ch}$ and $\tau_{0,co}$ are the proper time coordinates of the chaotic and the coherent source; $\delta\tau_{ch}$ and $\delta\tau_{co}$ their widths in proper-time; R_{ch} and R_{co} are the transverse radii; $L_\perp$ and L_η are the correlation lengths and L_τ is the correlation time. The tenth one is the chaoticity parameter.

To reduce the number of parameters we assume now that the widths in proper-time of both sources are vanishing ($\delta\tau_{ch} = \delta\tau_{co} = 0$); with this choice the results do not depend on the correlation time L_τ. The space-time distributions of the chaotic and coherent sources are then parametrized as:

$$f_{ch} \sim \delta(\tau - \tau_{0,ch}) exp\left(-\frac{x_\perp^2}{R_{ch}^2}\right) \tag{22}$$

$$f_{co} \sim \delta(\tau - \tau_{0,co}) exp\left(-\frac{x_\perp^2}{R_{co}^2}\right) \tag{23}$$

Note that the η dependence of $f_i(x)$ was neglected in equations (22) and (23). This corresponds to a boost-invariant ansatz of the source expansion.

The model contains now 7 independent parameters: $\tau_{0,ch}$, $\tau_{0,co}$, R_{ch}, R_{co}, $L_\perp$, L_η and the chaoticity parameter p_0 [4].

We will define, for convenience:

$$b = \frac{\tau_{0,ch}^2}{2L_\eta^2}, \quad R_L^2 = \frac{R_{ch}^2 L_\perp^2}{R_{ch}^2 + L_\perp^2} \quad \text{and} \quad \gamma_{12} = \frac{\tau_{0,ch}(m_{1\perp} - m_{2\perp})}{L_\eta^2 m_{1\perp} m_{2\perp}} \tag{24}$$

The single inclusive distribution will be a sum of a chaotic and a coherent term:

$$E\frac{1}{\sigma}\frac{d^3\sigma}{d^3k} = [p_0 s_{ch}(k) + (1-p_0)s_{co}(k)]E\left|\frac{1}{\sigma}\frac{d^3\sigma}{d^3k}\right|_{k=0} \tag{25}$$

$$s_{ch}(k) = \frac{m_\pi}{m_\perp} exp\left(-\frac{k_\perp^2 R_L^2}{2}\right) \tag{26}$$

[3] The parametrization for the primordial correlator, in the case of an expanding source, has to take into account that each source element is characterized not only by a correlation length but also by a four-velocity. Effects of the geometry of the source are considered by introducing the space-time distributions of the chaotic and the coherent component, $f_{ch}(x)$ and $f_{co}(x)$ respectively.

[4] The relative contributions of the chaotic and coherent component are determined by fixing the value of the (momentum-dependent) chaoticity parameter p at same arbitrary scale, e.g., $p_0 \equiv p(k=0)$ (cf. Eq. (32)).

$$s_{co}(k) = \frac{m_\pi}{m_\perp} exp\left(-\frac{k_\perp^2 R_{co}^2}{2}\right) \tag{27}$$

where $m_\perp$ is the transverse mass of the pions emitted and the momentum dependence of chaoticity parameter takes the form:

$$p_r = p(k_r) = \frac{p_0}{A_r}\ (r,s=1,2,3,4), \quad A_r = p_0 + (1-p_0)S_{rr} \tag{28}$$

$$S_{rs} = exp\left[-\frac{(k_{r\perp}^2 + k_{s\perp}^2)(R_{co}^2 - R_L^2)}{4}\right] \tag{29}$$

The magnitudes and phases of T_{rs}, ϕ_{rs}^{ch} and ϕ_r^{co} are:

$$T_{rs} = (1+\gamma_{rs}^2)^{-1/4} exp\left[-\frac{b(y_r - y_s)^2}{1+\gamma_{rs}^2} - \frac{(k_{r\perp} - k_{s\perp}^2)(R_{ch}^2 - R_L^2)}{8}\right] \tag{30}$$

$$\phi_{rs}^{ch} = \frac{b\gamma_{rs}}{1+\gamma_{rs}^2}(y_r - y_s)^2 - \tau_{0,ch}(m_{r\perp} - m_{s\perp}) - \frac{1}{2}\arctan\gamma_{rs} \tag{31}$$

$$\phi_r^{co} = -\tau_{0,co} m_{r\perp} \tag{32}$$

We proceed now to the the calculation of the correlation functions.

2 Calculations and Comparison with Experimental Data

The procedure for calculations consists in:
a) The phase-space is generated by Monte Carlo routines which take into account the experimental detection conditions mentioned in [11, 18, 19] and references there [5].
b)The simulated produced pions are registered with a determined $y, k_\perp$ and azimuth angle ϕ and from them one calculates the correspondent Q^2 value. The simulated particles are then selected in Q^2 bins, as described in the experimental papers quoted above.
c)The calculation of the functions T_{rs}, ϕ_{rs}^{ch} and ϕ_{rs}^{co} defined for an expanding source model is performed. From these results one is able to calculate the correlation function (and its integral for each defined bin), as determined by equations (4)-(6) and (18)-(20).

[5] Calculations taking into account a different simulated experimental window ($-2 < y < 2$, $0.125\ GeV < p_t < 1.5\ GeV$) show that the third and fourth order correlations calculations are more sensitive than the second order to the detection conditions in the range of $Q^2 < 0.5\ GeV^2$.

d)We use this procedure for second, third and fourth order correlation calculations, $C_2(Q^2), C_3(Q^2)$ and $C_4(Q^2)$.

To simplify the calculations we reduce the number of free parameters using the criterions presented in [16].

We assume that the chaotic and coherent components have the same transverse momentum spectrum, i.e., we choose $R_{co} = R_L$ [6]. R_L is constrained by the relation [7] $R_L = (\sqrt{\pi/2}) < k_t >^{-1}$. We also take $\tau_{ch,0} = \tau_{co,0} \equiv \tau_0$.

We are thus left with only four parameters: τ_0, R_{ch}, L_η and p_0.

These parameters have been investigated in the intervals[8]: $0.1 \leq p_0 \leq 1.0$; $0.8 < R_{ch} < 3.0$; $1.0 \leq \tau_0 \leq 2.4$ and $0.1 \leq L_\eta \leq 1.0$.

We will use the χ^2/ndf (ndf: number of degrees of freedom) method to evaluate the quality of the fits. We are looking for a general fit for all $C_i(Q^2)$ using the same group of parameters.

The procedure to select the groups of parameters for an overall fit was:

1) Calculation of χ^2 for each $C_i(Q^2)$ function for all parameters sets to delimit sectors in the parameters phase-space to be investigated. The groups of parameters which gave $\chi^2/ndf > 3$ for any calculated function were eliminated.

2) Search for regions of intersection in the parameters space for an overall description of the data. These regions were defined by minimizing χ^2/ndf for all three functions simultaneously [9] and imposing $\chi^2/ndf \leq 1.5$.

From 1) we concluded that there is a large number of parameter combinations which permit acceptable fits for $C_2(Q^2)$. The situation is quite different when one extends the search to $C_3(Q^2)$ and $C_4(Q^2)$.

Table 1 shows the groups of parameters we would like to comment on primarily. In all these groups $p_0 = 1$. It contains also the χ^2/ndf for each calculation.

Figure 1 shows the results for the best overall fit [10], corresponding to the group $N2$. In Table 2 we present the corresponding parameters and

[6]The meaning of this assumption depends on the value of p_0, which one obtains from the comparison between data and theoretical calculations. If $p_0 = 1$ the single and double inclusive cross sections do not depend on R_{co}.

[7]$< k_t >$ is taken from experiment.

[8]The steps used in the calculation to adjust the parameters are $\Delta R_{ch} = \Delta p_0 = \Delta\tau_0 = \Delta L_\eta = 0.1$.

[9]The best fits do not necessarily present the lowest value for χ^2/ndf of *each* function, since we look for regions in the parameter phase-space which minimize the χ^2/ndf for *all* three functions.

[10]We normalized the calculated correlation functions by choosing $C_i(Q^2) = 1$ for $Q^2 = 2.0GeV^2$ $(i = 2, 3, 4)$. The normalization factor is very close to one.

χ^2/ndf for each correlation function.

Table 1

sets	p_0	R_ch	L_η	τ_0	$C_2(Q^2)$	$C_3(Q^2)$	$C_4(Q^2)$
N1	1.0	1.7	0.2	1.1	1.35	1.23	1.49
N2	1.0	2.2	0.3	1.5	1.28	1.11	1.43
N3	1.0	2.5	0.3	1.3	1.31	1.12	1.41

Table 1: χ^2/ndf (last three colums) for each correlation function for the parameter sets $N1$,$N2$ and $N3$.

Table 2

function	p_0	R_{ch}	L_η	τ_0	χ^2/ndf
$C_2(Q^2)$	1.0 ± 0.01	2.2 ± 0.2	0.3 ± 0.01	1.5 ± 0.01	1.28
$C_3(Q^2)$	1.0 ± 0.01	2.2 ± 0.2	0.3 ± 0.01	1.5 ± 0.01	1.11
$C_4(Q^2)$	1.0 ± 0.01	2.2 ± 0.2	0.3 ± 0.01	1.5 ± 0.01	1.43

Table 2: The values of parameters and of χ^2/ndf corresponding to the best overall fit presented in Figure 1.

We could not find any combination with $p_0 < 1.0$, which would describe all correlation functions with the same goodness as when using $p_0 = 1.0$, which is the upper physical limit of chaoticity [11].

Calculations using $p_0 = 0.3$ and $R_{ch} = 1.7$ can produce good fits for $C_2(Q^2)$ ($\chi^2/ndf \leq 1.3$) in $0.2 < L_\eta < 0.7$ and in the entire τ_0 interval, but the minimum χ^2/ndf values for C_3 and C_4 are around 2.0 in the (very small) region of intersection of parameters. The behaviour of the C_2 function does not change even if the radius varies up to 2.5, but then there does not exist an intersection region of parameters (with $\chi^2/ndf \leq 1.5$) for C_3 and C_4. The calculations using $p_0 = 0.7$ presented almost the same behaviour. Values of $p_0 = 0.9$ or $p_0 = 1.1$ have also been investigated and did not provide an overall fit [12].

We found a clear tendency towards a common value of $L_\eta = 0.3$. The prefered range of the radius is $1.7 < R_{ch} < 2.2$.

[11] For completeness, calculations have been done also for $C_n(Q)$ besides $C_n(Q^2)$. The $C_n(Q)$ functions did not lead to new conclusions about the choice of parameters, they were in general agreement with the behaviour of $C_n(Q^2)$. The group $N2$ also describes the data in Q. The values of χ^2/ndf for these functions are also smaller than 1.5 but one has again to bear in mind that the error bars are here much bigger and therefore one has to be careful with the interpretation of these results.

[12] To investigate the sensitivity of the fits on p_0, an analysis also for $p_0 = 1.5$ was made in a bigger parameter space. The range of τ_0 was amplified up to 7.0 and that of R_{ch} up to 10.0. The lowest χ^2/ndf for each correlation function varied between 2.9 and 6.9.

Figure 1

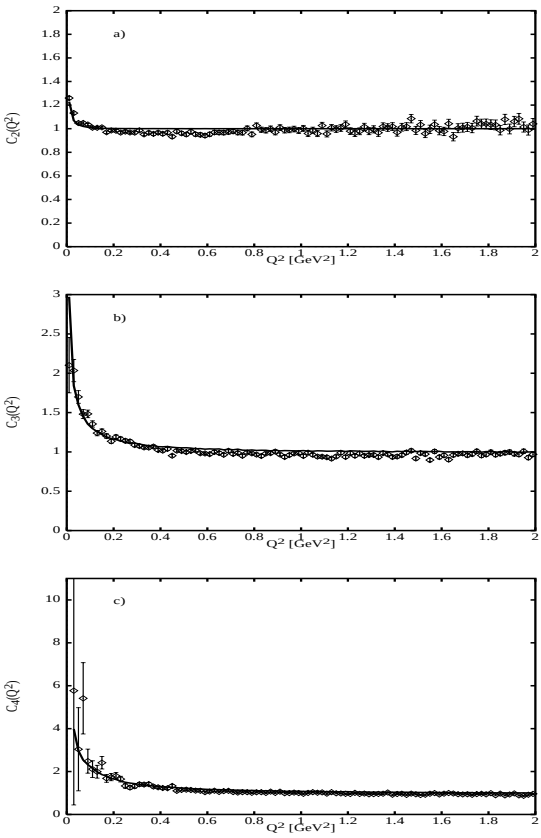

Figure 1: The two-, three- and four-particle correlation functions in Q^2 calculated using the space-time model defined in the text (continous lines), with the parameters $N2$ (see Table 1) and comparison with experimental data from [11].

The range of τ_0 seems to be connected with that of the radius. One gets the best fits for $R_{ch} = 1.7$ with $\tau_0 = 1.1$ and for $R_{ch} = 2.2$ with $\tau_0 = 1.5$ (see Table 1).

As already mentioned, the number of groups of parameters which provide an acceptable fit for $C_2(Q^2)$ is much bigger than the number of groups which provide an acceptable general fit. This is exemplified in Figure 2. This figure should also also clarify the method used in this work, which differs from the one used in [20], where the parameters obtained from a fit of C_2 data were used to "predict" C_3.

For the results in Figure 2 we used: $p_0 = 0.7$, $R_{ch} = 1.8$, $\tau_0 = 2.2$ and $L_\eta = 0.5$. The corresponding χ^2/ndf values for C_2, C_3 and C_4 functions are: 1.30, 7.05, 1.83.

Figure 2

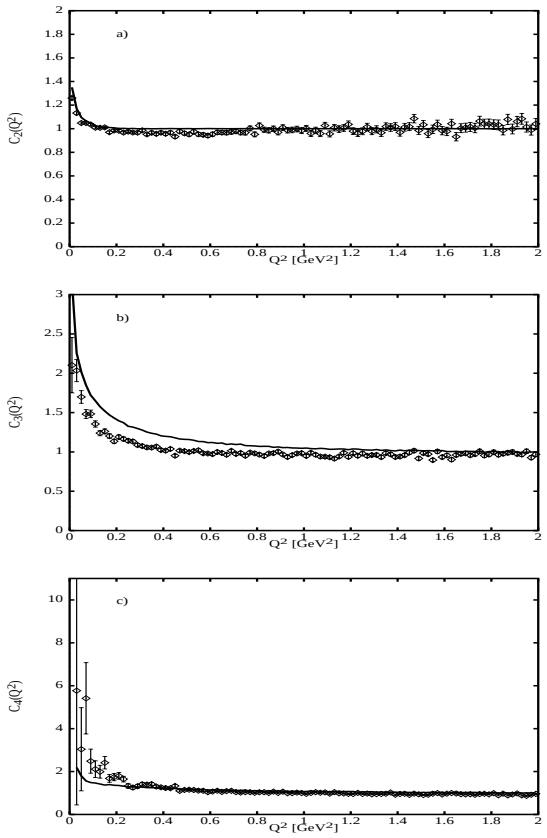

Figure 2: The same calculation as in Figure 1 using the other set of parameters as defined in the text. The figure shows that parameters which produce acceptable fits for $C_2(Q^2)$ do not necessarily give good overall fits.

3 Discussion and Conclusions

Our main conclusion is that in the frame of a model based on quantum statistical principles and a space-time picture of an expanding source, a general description of the higher order correlations data with the same parameters [13], as those appearing in the first two correlation orders, is possible. The assumption of a gaussian form for the density matrix is

[13] Given the simplifications made above resulting in the reduction of the number of parameters from a minimum of 10 to only 4, the quantitative estimates obtained above for the radius, correlation length, life-time and chaoticity, although reasonable from the physics point of view, must not be overemphasized, the more so that the data on which these estimates are based, have large errors.

consistent with the data.

A similar but weaker conclusion was reached in [15] . In [15] it had been shown that the gaussian form of the density matrix is robust enough to resist attempts of falsification [8] [14].

On the other hand in [8] and [15] the momentum-space approach was used, the currents were assumed to be real and no simultaneous fit of all correlation functions has been performed. Similar caveats apply to [11] where an analysis of the same NA22 data as those investigated in the present paper was presented and where only "marginal" agreement with the simplified quantum optical model of [12, 13] was found. The fact that in the present work we could fit the same data supports the space-time approach and the necessity of simultaneous fit.

Besides the fact mentioned already that correlators in momentum-space are associated with a four dimensional "radius" which has no clear physical interpretation, the space-time approach and the momentum-space approach differ also from a purely mathematical point of view. In [12, 13, 15] the Q dependence is postulated from the beginning while in the present paper, as in [16], it results from a complex process of integration.

In [20] the same momentum-space model ([12, 13, 15]) as that used in [11] was applied and compared with UA1-collaboration data. This time a new technique for estimating the correlation data was used but only second and third order correlations were considered. At first the best fit parameters set for the second order correlation data was established and then used to *predict* the third order correlation function, which was found to disagree with the measured one. Given the insensitivity of of the fit parameters found by us on the C_2 function, this result is not surprising and the fitting procedure used in [20] has to be qualified as well as the procedure used in [11]. Furthermore the general reservations expressed above about the momentum-space approach apply here again.

One may put the question why it is necessary to invoke higher order correlations to constrain the source parameters whereas the presence of a gaussian density matrix implies that the first and second moment of the current distribution, $I(k)$ and $D(k_1, k_2)$, determine all higher order correlations [15].

[14] For a more detailed discussion of this issue cf. also the comments preceding the reprinted paper by Neumeister et al. in [21].

[15] There is of course the fact that the phases ϕ of eq.(13) enter in different combinations in the various correlation functions. This is true both in the momentum-space approach [12, 13, 15], as well as in the space-time approach. In the application to data [8] and [11] of the quantum optical approach this complication was "circumvented" by assuming that the fields are real.

In the applications of the space-time approach [17] however one has also to take into account that due to the limited statistics, most experimental BEC data including those analyzed in the present paper give the correlations in one single variable, Q. On the other hand, the correlation function C_2, for instance, depends on 6 variables: the three momenta of the pions of the pair, $\vec{k}_1$ and $\vec{k}_2$ [16]. Thus a large amount of information is lost due to the integration that projects out the Q dependence (cf. (5) and (6)). This is a fortiori true for higher order correlations. Therefore phenomenologically higher order correlation data can play an important role in constraining the source parameters.

On the other hand the fact that we were able to account for the data even within this simplified approach, proves that there are still many degrees-of-freedom not used at the present level of theory/data comparison so that the challenge of disproving the gaussian density matrix will remain a hard task for a long time ahead.

[16] In the case of symmetries of the source geometry, the number of independent variables is slightly reduced: e.g., for the boost-invariant azimuthally symmetric expanding source discussed here, there are four independent variables.

References

[1] V. P. Kenney et al., Nucl. Phys. B144 (1978) 312.

[2] M. Althof et al, TASSO Coll., Z. Phys. C30 (1986) 355.

[3] I. Juricic et al, MARK II Coll., Phys. Rev. D39 (1989) 1.

[4] J. L. Baily et al, NA23 Coll., Z. Phys. C43 (1989) 341.

[5] A. Breakstone et al., Mod. Phys. Lett. A6 (1991) 2785.

[6] V. V. Aivazyan et al., EHS/NA22 Coll., Z. Phys. C51 (1991) 2785.

[7] T. Akesson et al., AFS Coll., Z. Phys. C36 (1987) 517.

[8] N. Neumeister et al., UA1 Coll., Phys. Lett B275 (1992) 186.

[9] I. V. Ajinenko et al., EHS/NA22 Coll., Z. Phys. C61 (1994) 567.

[10] N. M. Agababyan et al., EHS/NA22 Coll., Phys. Lett. B332 (1994) 458.

[11] N. M. Agababyan et al., EHS/NA22 Coll., Z. Phys. C68 (1995) 229.

[12] R.M.Weiner, Phys. Lett B232 (1989) 278; B242 (1990) 547.

[13] M. Biyajima et al., Prog. Th. Phys. 84 (1990) 931.

[14] P. Carruthers, H. C. Eggers and Ina Sarcevic, Phys. Lett. B254 (1991) 258.

[15] R. Plümer, I. V. Razumov and R. M. Weiner, Phys. Lett B286 (1992) 335.

[16] I. V. Andreev, M. Plümer, B. R. Schlei and R. M. Weiner, Phys.Lett. B316 (1993) 583; Phys. Rev. D49 (1994) 1217.

[17] I. V. Andreev, M. Plümer and R. M. Weiner, Int. Jour. Mod. Phys. A, vol. 8, n. 26, (1993)4577.

[18] M. Adamus et al., EHS/NA22 Collaboration, Z. Phys. C39 (1988) 311.

[19] N. M. Agababyan et al., EHS/NA22 Collaboration, Z. Phys. C59 (1993) 195.

[20] H. C. Eggers, B. Buschbeck and P. Lipa, Phys Rev. Lett. 79 (1997) 197.

[21] R.M.Weiner, Bose Einstein Correlations in Particle and Nuclear Physics, John Wiley & Sons, 1997.

[22] N. M. Agababyan et al., EHS/NA22 Collaboration, Z. Phys. C71 (1996) 405.

Appendix 1

The experimental observables and measurements: some definitions

1 Phase Space Variables

1. **space-time and system coordinates** There are three spacial coordenates and one time coordenate. The 'logitudinal' or 'parallel' direction denotes the space variable in the beam direction. (In the figure, P: projectile and T: Target)

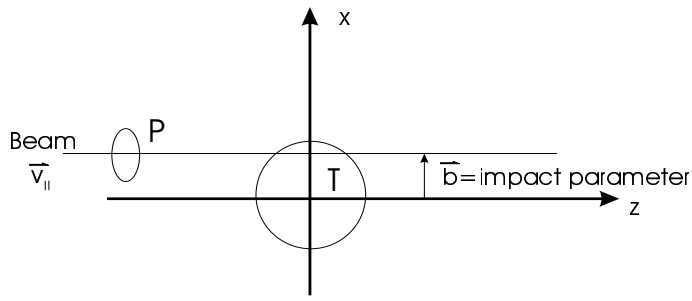

2. **four momentum**

   The four-momentum of a particle in four-dimensional space-time is: $p^{\mu} = (p^0, \vec{p})$, where $p^0 = E$, as usual for relativistic energies. The four-momentum is a time-like vector with normalization: $(p^0)^2 - (\vec{p})^2 = m^2$.

3. **transverse momentum and transverse mass**

$$p_{\perp} = p_t = \sqrt{p_y^2 + p_x^2} \tag{1}$$

$$m_{\perp} = m_t = \sqrt{m^2 + p_{\perp}^2} \tag{2}$$

4. **rapidity**

$$y = \frac{1}{2} ln \left(\frac{E + p_z}{E - p_z} \right) \tag{3}$$

5. **phase space element**

$$E = \sqrt{p^2 + m^2} = \sqrt{p_{\parallel}^2 + p_t^2 + m^2}$$

$$\int d\vec{p} = \int_{\phi} p_t . dp_t . d_{\phi} . dp_{\parallel} = \pi d(p_t^2) . E . dy \tag{4}$$

2 Data Terminology

1. **differencial cross section**

   One considers the expression $d^3\sigma/(d\vec{p}/E)$ as invariant cross section because $d^3\vec{p}/E$ is a relativistic (Lorentz) invariant. Using the relation (4) one can write the differencial cross-section for the creation of one particle with impulse $\vec{p}$ and energy E:

$$\frac{Ed^3\sigma}{d\vec{p}} = \frac{Ed^2\sigma}{\pi d(p_t^2)dp_{||}} = \frac{d^2\sigma}{\pi d(p_t^2)dy} \tag{5}$$

   The analysis of the creation of the particles (their energy) in the beam direction through the defined 'rapidity' variable, is called rapidity distribution data (or dN/dy).

2. **transverse momentum distribution**

   Transverse-momentum spectra are usually presented in the form:

$$E\frac{d^3\sigma}{d\vec{p}} \sim \frac{1}{p_\perp}\frac{d^2\sigma}{dp_\perp d_y} \tag{6}$$

3. **Bose-Einstein correlation**

   The two-pion correlation function has experimentally the form:

$$C(p_1, p_2) = \frac{N_2(p_1, p_2)}{N_1(p_1)N1(p_2)} \tag{7}$$

   where the p_i are the four-momenta of the pions and N_1 and N_2 are the single and double inclusive distribution functions, respectively. For more information about this topic, see Part II of this dissertation.

Appendix 2

The measurements and the stages of the reaction

A summary of the proposals to associate measurements with the different stages of the reaction [1]:

1. To get information about the **initial conditions** of the system one should work on the interpretation of the global event features measurements.

   A significant part of the effort in the experiments was spent on investigating global features of nuclear interactions as cross-sections, energy distributions and particle production. The questions of what happens to nuclei passing through each other at very high energies (stopping) and what happens to the energy lost (energy and particle flow) are the subject of this data category. In order to specify, under this category are: total cross sections, differential cross-sections, transverse energy production, (pseudo-)rapidity distributions, baryon rapidity distributions, and the last one, energy density, baryon density and scalling behaviour.

   From these data one tries to resconstruct, in a model dependent way, the initial dimensions of the fireball and the impact parameter of the collision.

2. Signatures of **quark gluon plasma** are supposed to be probes from the very early time of the reaction, these probes should not interact with the system until they reach the detectors. Direct photons and lepton pairs could be such observables [2] -[4]. The hot matter should emit them and they would not be altered by latter interactions. They contain information about the space-time geometry of the fireball, once they are created during the whole process, but not about the constituints of hot nuclear matter.

   The suppression of the resonance J/Ψ was also proposed as a signature based on the argument that its 'melting' would be possible only in a deconfined scenario [5]. 'Jet quenching'- the way the jets lost energy [6], massive photons [7] and 'stable' strange matter [8] [9] are also supposed to be signals from a deconfined environment.

   The detection of free quarks would be the only definite sign of quark gluon plasma formation. This is not possible.

3. A **first order phase transition** is characterized by constant temperature in an significant interval of energy. Some authors proposed p_t and energy density and their interdependence [10, 11] to analyze it [1]. Details about a phase trasition and hadronization also could come from strange particle production, once they should be abundantly produced in plasma and the number of the surviving ones depends on the hadronization process and expansion [12]. Phase transition also influence the life-time of the fireball, which can be studied in the analysis of Bose-Einstein correlation [13] [14].

4. Finally the system should expand and cool down as a **hadron gas**. As mentioned before, p_t spectra should reflect the expansion of the fireball and more information about the dimensions and evolution of the system should be possible to get from Bose-Einstein correlation data analysis. They bring also information about the dimensions of the system at **freeze-out** [15]-[18].

[1] One important point to remark is that the association of the shape of p_t particle spectra with the temperature of the system when the particle as emmited is only possible when the system presents small tranverse expansion. Only in this case one can use the expression $< p_t >= \int exp(-E/T)\ dp_t$, which is used to make this interpretation. In other cases the energy E has to be corrected with a $(-p_\mu u^\mu)$ component and the interpretation is not more valid. This aspect is frequently neglected in the literature.

References

[1] H. R. Schmidt and J. Schukraft, Mod. Phys. D

[2] E. Schuryak, Phys. Lett. B78 (1978) 150.

[3] K. Kajantie and H. I. Miettinen, Z. Phys. C9 (1981) 341.

[4] L. D. McLerran and T. Toimela, Phys. Rev. D31 (1985) 545.

[5] T. Matsui and H. Satz, Phys. Lett. B178 (1986) 416.

[6] M. Gyulassy and M. Plümer, Phys. Lett. B243 (1990) 432.

[7] H. A. Weldon, Phys. Rev. Lett. 66 (1991) 293.

[8] C. Greiner, P. Koch and H. Stöcker, Phys. Rev. Lett. 58 (1987) 1825.

[9] C. Greiner et al., Phys. Rev. D38 (1988) 2797.

[10] L. Van Hove, Phys. Lett. B118 (1982) 138.

[11] E. V. Shuryak and O. V. Zirhov, Phys. Lett. B171(1986)99.

[12] K. S. Lee and U. Heinz, Z. Phys. C34 (1989) 425.

[13] S. Pratt, Phys. Rev. D33 (1986) 1314.

[14] G. Bertsch, M. Gong and M. Tohyama, Phys. Rev. C37 (1988) 1896.

[15] S. Pratt, Phys. Rev. Lett. 53 (1984) 1219.

[16] B. Lorstadt, Int. J. Mod. Phys. A4 (1989) 2861.

[17] H. Boal, C. Gelbke and B. Jennings, Rev Mod. Phys. 62 (1990) 553.

[18] M. G. Bowler, Z. Phys. C46 (1990) 305, C39 (1988) 81.

Zusammenfassung

Das Ziel dieser Arbeit ist die Untersuchung von starkwechselwirkenden Systemen, die in hochenergetischen Stößen erzeugt worden sind. Weil die Theorie von Quarks und Gluonen - Quantenchromodynamik (QCD) - nicht ausreicht, die gesamte Entwicklung von starkwechselwirkender Nuklearmaterie unter extremen Bedingungen zu beschreiben, muß man phänomenologische Methoden benutzen.

In **Teil I** wurden **Kern-Kern Stöße** unter Anwendung einer exakt (3+1)-dimensionalen numerischen Lösung der relativistischen Gleichung der Hydrodynamik untersucht. Ich präsentiere ein Modell, genannt HYLANDER-PLUS, zur Simulation der hochenergetischen Reaktionen. Damit ist man in der Lage, die Produktion von 16 verschiedenen Hadronen und die Produktion von Photonen/Leptonen zu berechnen, Anfangsbedingungen für totales und partielles 'Stopping' zu simulieren und die hydrodynamischen Gleichungen unter Anwendung von zwei verschiedenen Zustandsgleichungen (EOS) zu lösen. Die Simulationen, die unter Anwendung des Grundmodells gemacht worden sind, waren in all diesen Aspekten begrenzt.

Das neue Modell wurde angewendet, um Daten aus 4 Reaktionen zu beschreiben: $Au + Au$ bei 11 $GeV/nucleon$; $S + S$, $Pb + Pb$ und $S + Au$ bei 200 $GeV/nucleon$.

In der Simulation der $Au+Au$ Reaktion sind die Parameter in der Zustandsgleichung die einzigen freien Parameter. Zwei verschiedene EOS sind benutzt worden: Die eine beinhaltet einen Phasenübergang vom Quark-Gluon-Plasma zur hadronischen Phase und die andere zieht ein Resonanzengas im Betracht. Man kann zeigen, daß die Existenz eines Phasenübergangs die Form der Datenspektren beeinflußt. Die experimentellen Daten aus dieser Reaktion konnten durch die Simulation beschrieben werden, zusätzlich konnte die Produktion von Schwerbaryonen und Anti-Schwerbaryonen vorhergesagt werden. Manche vorgeschlagenen 'QGP Signatures' sind überprüft worden.

In einigen Experimenten wurde beobachtet, daß bei niedrigen p_t die Produktion von π^- in Relation zur Produktion von π^+ anstieg. Die Reaktionen $S+S$, $Pb+Pb$ and $Au+Au$ wurden simuliert und die Ergebnisse der Simulationen - Pionenspektren - mit den Messungen verglichen. In dieser Untersuchung wurde gezeigt, daß die gängige Interpretation, die auf dem Coulomb-Effekt basiert, nicht befriedigend ist, und es wird eine andere Erklärung für den Anstieg der π^- Produktion vorgeschlagen. Grundlage für diese Erklärung ist der Zerfall von Resonanzen.

Mit diesem Modell konnten die Daten für die Photonenproduktion der $S + Au$ Reaktion beschrieben werden. Auch für $Au + Au$ und $Pb + Pb$ Reaktionen wurde die Photonenproduktion berechnet. Entgegen der allgemeinen Erwartung ergaben sich aus der Simulation für $Au + Au$ experimentell beobachtbare Quoten. Aus diesen Ergebnissen sind die Zeit-Raum-Entwicklung des Feuerballs und die entsprechende Photonenproduktion für jede Phase gezeigt worden. Dieser Aspekt ist für die Anwendung der Photonenproduktion als 'Quark-Gluon-Plasma signature' sehr wichtig.

Die Hauptschlußfolgerung aus Teil I ist, daß die hydrodynamischen Annahmen mit den experimentellen Daten aus hochenergetischen Kern-Kern-Stößen weitgehend übereinstimmen. Die exakt (3+1)-dimensionale numerische Lösung der relativistischen hydrodynamischen Gleichungen ist ein wesentliches Instrument, um die stark wechselwirkenden Vielteilchensysteme und die hadronische Vielteilchenproduktion zu beschreiben.

In **Teil II** dieser Arbeit wurden die Raum-Zeit-Aspekte der hochenergetischen **Hadron-Hadron Stöße** durch Bose-Einstein-Korrelationen analysiert. Es wurden neue Daten über Korrelationen von Pionen zweiter, dritter und vierter Ordnung aus $\pi^+ - p$ und $K^+ - p$ Reaktionen bei 250 GeV/c untersucht.

Für diese Untersuchung wurde ein quantenstatistisches Zeit-Raum-Modell benutzt. Die experimentellen Daten konnten mit 4 Parametern beschrieben werden, die für alle Ordnungen von Korrelationen dieselben Werte haben.

Die Hauptschlußfolgerung dieses Teils der Arbeit ist, daß eine Zeit-Raum-Behandlung der Quelle in einem quantenstatistischen Modell möglich ist. Das bestätigt die Annahme der Gaußschen Form für die Dichtematrix. Diese Ergebnisse sind verschieden von den bisher veröffentlichten, die keine expliziten Zeit-Raum Konzepte für Quelle und Korrelatoren enthalten.

Summary

The aim of this dissertation is the investigation of strongly interacting systems created in high energy collisions. Since the theory of quarks and gluons - QCD - is not able to describe the whole development of strongly interacting nuclear matter in extreme conditions, one has to use phenomenological methods to study it.

In **Part I** an investigation on **nucleus-nucleus collisions** using an exact (3+1) dimensional numerical solution of the relativistic hydrodynamical equations is made. I present a model, which I call HYLANDER-PLUS, to simulate the high energy reactions. Using this model one is able to calculate the production of 16 types of hadrons and the production of photons/leptons, one can simulate initial conditions for collisions with partial or full stopping and one can solve the hydrodynamical equations using different kinds of equations of state (EOS). This model is based on a previous version, which was very restricted in all above mentioned aspects.

The model has been applied to describe data from four reactions: $Au + Au$ at 11 $GeV/nucleon$; $S + S$, $Pb + Pb$ and $S + Au$ at 200 $GeV/nucleon$.

In the simulation of $Au+Au$ reaction the only free parameters are the ones which enter in the equation of state. Two different EOS were used, one containing a phase transition of nuclear matter from the quark gluon plasma phase to the hadronic phase and one considering a resonance gas. The influence of the existence of a phase transition on the shape of data spectra is analyzed. The model describes the already published data and predictions for heavy baryons and heavy anti-baryons production were made. Some of the proposed quark gluon plasma signatures have been checked.

An enhancement of π^- production relative to π^+ production at low p_t has been observed in certain heavy ion reactions. An study about this enhancement is made for $S+S$, $Pb+Pb$ and $Au+Au$ reactions. In this study I show that the proposed interpretation for the enhancement, based on the Coulomb effect, was not satisfactory and an alternative explanation for this enhancement is presented. This explanation is based on resonance decays.

A description of photon production data for the $S + Au$ reaction is obtained. Predictions for photon production in $Au+Au$ and $Pb+Pb$ are also presented, and, contrary to expectations, the simulation for $Au+Au$ also produced experimentally observable rates. From these results the

space-time development of the fireball and the corresponding photon production for each phase of the reaction process are shown. This study is important for the use of photon production data as a quark gluon plasma signature.

The main conclusion of Part I is that the hydrodynamical assumptions are in general agreement with the experimental data for high energy nucleus collisions. The exact (3+1) dimensional numerical solution of the relativistic hydrodynamic equations is an essential instrument to describe strongly interacting many-particle systems and hadronic multiparticle production.

In **Part II** space-time aspects of **hadron-hadron collisons** at high energies using Bose-Einstein correlations are analized. New data on two, three and four correlated pions for $\pi^+ - p$ and $K^+ - p$ reactions at 250 GeV/c are studied.

The model is a quantum statistical space-time approach. One shows that the data for second, third and fourth order of correlations can be described with a reduced group of parameters (4), which have the same values for all orders.

The main conclusion of this part is that an expanding source treatment in the context of a model based on quantum statistical principles is possible, confirming the gaussian form assumption for the density matrix. These results are different from the ones published before, which did not use explicit space-time concepts for source and correlators.

Danksagung

An dieser Stelle möchte ich allen danken, die in irgendeiner Form zum Gelingen dieser Arbeit beigetragen haben:

• Prof. Dr. R. M. Weiner für die Aufnahme in seine Arbeitsgruppe, die sehr interessante Aufgabenstellung und viel Geduld.

• den ehemaligen Mitgliedern der Arbeitsgruppe Dr. habil. Michael Plümer und Dr. Udo Ornik für die offenen Ohren und für die wichtigen Tips.

• 'Super' Frau Webel für die unersetzliche Begleitung in dieser Zeit.

• Prof. Dr. Peter Thomas, Prof. Dr. Stephan Koch und den Mitgliedern der Halbleiterphysik-Arbeitsgruppe für die tägliche Unterstützung, besonders Klaus und Bernd für die unendliche Aufmerksamkeit.

• Dr. Axel Koch (in memoriam) und den Mitarbeitern des Hochschulrechnenzentrums für die Hilfe und Ratschläge in 'Soft-' und 'Hard-' 'ware'- Angelegenheiten.

• Herrn Claus und Inge für die außergewöhnliche deutsche Familie, die mich 'adoptiert' hat.

• Nelson und Marly - meine Eltern - für das Vertrauen in meine Träume. Alexandre und Cyntia - meine Geschwister - für die 'Komplizenschaft' und für die 'Neuigkeiten'.

• Pi, Edson, Christiane und Matthias, Miguel, Jens, Annette, Anja und Michael, Gabriela, Janet, Irmchen, Peter, Ulli, Frau Just, Karl-Heinz, Adriana und Jan, die mit mir durch 'dick und dünn' während dieser viereinhalb Jahre gegangen sind und meinen Alltag versüßt haben.

• Frank für die fantastischen Überraschungen.

• CNPq - Brasil, für die finanzielle Unterstützung.